



ORIGINAL ARTICLE

Response surface methodology optimization of dynamical solutions of Lie group analysis for nonlinear radiated magnetized unsteady wedge: Machine learning approach (gradient descent)



M. Dinesh Kumar^{a,1}, N. Ameer Ahammad^b, C.S.K. Raju^{a,c}, Se-Jin Yook^c, Nehad Ali Shah^{d,1}, Sayed M. Tag^{e,*}

^a Department of Mathematics, GITAM School of Science, GITAM-Bangalore, 562163, India

^b Department of Mathematics, Faculty of Science, University of Tabuk, P.O. Box 741, Tabuk 71491, Saudi Arabia

^c School of Mechanical Engineering, Hanyang University, 222 Wangsimni-ro, Seongdong-gu, Seoul 04763, Republic of Korea

^d Department of Mechanical Engineering, Sejong University, Seoul 05006, South Korea

^e Center of Research, Faculty of Engineering, Future University in Egypt, New Cairo 11835, Egypt

Received 29 March 2023; revised 25 April 2023; accepted 3 May 2023

Available online 16 May 2023

KEYWORDS

Nanofluid;
Response surface method;
Radiation;
Hybrid nanofluid;
Ternary hybrid nanofluid;
Lie group transformations;
Sensitivity analysis;
Machine learning with simple linear regression;
Gradient descent method

Abstract When a consistent transverse magnetic field and heat radiation are present, the flow of boundary layer, Over porous wedge nanofluids, hybrid nanofluids, and ternary hybrid nanofluids have been studied., Water as base fluid, Hybrid nanofluid, Ternary Hybrid nanofluid, and nanofluid cases containing Case-1 Polyethylene Glycol-Water + AA7072, Case-2 Zirconium oxide + A A7072 + Polyethylene Glycol-Water Case-3 Magnesium oxide + Polyethylene Glycol-Water + AA7072 + Zirconium oxide is taken into consideration. Runge-Kutta (4th order) with the Shooting technique is used to solve the governing equations expressed in terms of Odes. For various values of the relevant parameters, the approximate relationship between temperature, velocity, rate of heat transfer, and shear stress at the wedge is depicted visually. It is found that the Nusselt number transfer rate is more in Ternary hybrid nanofluids than Hybrid and Nanofluids and the Skin friction rate is more in Hybrid nanofluids than in Ternary and Nanofluids. Table 9 shows the comparative study with recently published paper numerically having a good agreement of results. RSM method is useful to find the optimization conditions values based on the key factors that impact the

* Corresponding author.

E-mail addresses: anaudalur@ut.edu.sa (N. Ameer Ahammad), rchakrav@gitm.edu (C.S.K. Raju), ysjnuri@hanyang.ac.kr (S.-J. Yook), elsayed.research@fue.edu.eg (S.M. Tag).

¹ These authors contributed equally to this work and are co-first authors.

Peer review under responsibility of Faculty of Engineering, Alexandria University.

Response Function. Simple linear regression machine learning with the Gradient descent method has been applied to some of the dimensionless parameters this method predicts the truth values accurately.

© 2023 THE AUTHORS. Published by Elsevier BV on behalf of Faculty of Engineering, Alexandria University. This is an open access article under the CC BY-NC-ND license (<http://creativecommons.org/licenses/by-nc-nd/4.0/>).

1. Introduction

A series of ongoing alterations and transformations occurring on the expanded space of dependent and non-dependent variables and the equation parameters is referred to as a Transformation of a partial differential equation using a Lie group. The Lie group approach using infinitesimal changes is a traditional technique to reduce the similarity of non-linear differential equations. After similarity analysis, fewer variables govern PDE, which converts them to ODE. In dynamical systems without linearity, mainly when it manifests as deterministic done by chaos, a particular type of the most effective, complex, and systematic method for creating similarity transforms is the Lie group transformation, called the scaling group transformation as well. The group-invariant starting and boundary value problem solutions are the widely used solutions for similarity for the scaling group of changes. Numerous studies have used scaling group techniques [1–3]. The mixture of a single nanoparticle with a base fluid is known as a Nanofluid; Nanoparticle size is less than 100 nm; Hybrid nanofluid is a mixture of more than one nano properties with a base fluid. Due to these fluids' enhancement of heat transfer rate, it will be helpful for industrial purposes by using the study of [4–5]. The conclusion is that the thermophoresis, Lewis, and Brownian motion numbers considerably flow field effects of the nanoparticle volume fraction and temperature profiles studied by Abdul et al. [6] through crossing a porous, vertically stretched surface with a nanofluid's boundary-layer flow with a scaling group transformation. Marangoni convection flow and heat transport are impacted by radiation. in non-Newtonian pseudo-plastic nanofluids with variable thermal conductivity. Lin et al. [7] analyze and discuss temperature and velocity fields' effects on the precise power-law number, radiation number, and solid volume fraction. Bilal Ahmad et al. [8], Maxwell nanoparticles with different flow characteristics were studied for thermal diffusion. The findings of Lie group simulations demonstrate how the mass transfer parameter and buoyancy constant predict a reduction in velocity while the opposite acceleration pattern is observed. Entropy production in a combining suction and injection, boundary layer flow with triple diffusive convective heating, and multi-linear regression of a hybrid Eyring-Powell nanofluid flow that is erratic over a permeable surface. This invention, Lie group transformations, was created by the researchers listed below [9–10]. A Lie group analysis of the effects of nanofluids with embedded carbon nanotubes on the free convective radiative flow, the magnetic field, and Navier slip this investigation has been done by Sreenivasulu al. [11]. It is discovered that the nanofluid velocity falls as the slip factor increases. The temperature rises with improved thermal energy generation, but the heat flux falls. and storage. Biglarian et al. [12] investigated heat transport in permeable channels using various water-based nanofluids under unstable conditions. When the

expansion ratio was increased, the heat transfer rate fell but The Hartmann number, Reynolds number, and volume percentage of nanofluids all rose. when there was an external magnetic field. Hamid Maleki et al. [13], according to research on the flow and heat transmission in Nanofluids over porous surfaces, non-Newtonian, the non-Newtonian nanofluid performs better at heat transfer versus the impermeable plate and the Newtonian nanofluid for injection. According to Uddin et al. [14], magnetic field effects minimize skin friction and increase the heat transfer rate in a computational simulation of the Newtonian fluid on a heating surface and the Slip flow of a nanofluid in MHD across a radiating plate. According to a study by Mahabaleshwar et al. [15], the flow's effects happen faster and accelerated with a decrease in the inverse Darcy number due to Mass transfer and hydromagnetic hybrid nanofluid flow created by porous stretching sheets, Navier's slip and chemical reaction and more potent suction, which directly reduces skin friction. According to a study by Haffez et al. [16] on dual solutions for convergent channels with dissipative heat transport and water-based hybrid nanofluids, current findings will be used in the polymer industry, biomedical research, petroleum science, and other fields. According to Ahmad et al. [17], Fluid movement near a hyperbolic tangent in the presence of heat was studied using Lie groups; the local Nusselt area value decreases as the thermal radiation parameter is raised, it is concluded by Researchers [18–19] have examined the results of heat transmission, the flow of hybrid nanofluids across a sheet that is contracting and expanding with the consistent shear flow, and the flow on a stretching sheet. Bhattacharya et al. [20] created a statistical and numerical approach to describe the flow properties of a copper and graphene nanoparticle-containing Maxwell hybrid nanofluid. Exact multiple solutions of 2-D bidirectional moving plate micropolar hybrid nanofluid flow with heat transfer, Exact multiple solutions of second-degree nanofluid slip flow and heat transport in the porous medium, and Exact multiple solutions for micropolar slip flow and heat transfer of a bidirectional moving plate investigation have all been studied by the researchers [21–25]. Ternary hybrid nanofluids flow on a spinning disc with nonlinear thermal radiation, Ternary hybrid nanoparticles simultaneously on thermal radiative flow configured by Darcy-Forchheimer porous surface, and thermal characteristics of nonlinear convection and radiation for the flow of tri-hybrid nanofluids over stretchable surface with energy source [26–28]. An Eigenvalues Approach for a Two-Dimensional Porous Medium Based Upon Weak, Normal, and Strong Thermal Conductivities was explored by the researchers [29–30] as well as the exponential type decay for solutions in a dipolar elastic body.

The flow regulating equations are subjected to a scaling group transformation method in the current research, and the resulting ODEs are subsequently numerically solved using the shooting technique (RK-4thorder). Graphs are used to dis-

play the results of simulations. The validity of computational results is confirmed by existing research. The use of RSM to optimise the rate of heat transfer and machine learning with the gradient approach is another innovative aspect of this study.

2. Mathematical Formulation:

In a two-dimensional, MHD unstable environment, the Darcy flow of an incompressible nanofluid across a porous wedge sheet (see Fig. 1). The temperature becomes constant both within and outside the wedge, T_w and T_∞ in relation to magnetic strength B_0 applied in a straight line to the y-axis. The following three cases involved the Ternary Hybrid Nanofluid of Polyethylene Glycol and Water into Nanoparticles of AA7072, Zirconium Oxide, and Magnesium Oxide. case-1 Base fluid containing nanoparticle AA7072, case-2 Base fluid containing ternary hybrid nanoparticles AA7072, zirconium oxide, and magnesium oxide, and case-3 Base fluid containing ternary hybrid nanoparticles AA7072. The suspended nanoparticles and the base fluid (Polyethylene Glycol-Water) are in thermal equilibrium. The study's [31–32], Table 1 lists the thermophysical characteristics of the nanofluids. The porous wedge is assumed to be transparent and in thermal equilibrium with the nanofluids. A wedge sheet that is non-reflecting, absorbent, and preferably transparent detects an intensity flux of incident radiation q''_{rad} . The thermal flux passes through the plate and is absorbed in a fluid with a nearby high absorption coefficient. The justification for the induced magnetic field created by fluid motion is $B = (0, B_0, 0)$ by Kandasamy et al. [33–34] findings used to define the momentum and energy equations on the premise that the influence of fluid polarisation is insignificant.

$$\frac{\partial v}{\partial y} + \frac{\partial u}{\partial x} = 0 \quad (1)$$

$$v \frac{\partial T}{\partial y} + u \frac{\partial T}{\partial x} + \frac{\partial T}{\partial t} = \frac{1}{(\rho c_p)_{hmf}} (k_{hmf} \frac{\partial^2 T}{\partial y^2} - \frac{\partial q''_r}{\partial y} - Q_0(T - T_\infty)) \quad (2)$$

$$v \frac{\partial u}{\partial y} + u \frac{\partial u}{\partial x} + \frac{\partial u}{\partial t} = \frac{1}{\rho_{hmf}} \left[\left(\frac{\partial U}{\partial t} + U \frac{\partial U}{\partial x} \right) \rho_{hmf} + \mu_{hmf} \frac{\partial^2 u}{\partial y^2} + (\rho \beta)_{hmf} g (T - T_\infty) \sin \frac{\Omega}{2} - \left(\sigma B_0^2 + \frac{v_{hmf}}{K} \rho_{hmf} \right) (u - U) \right] \quad (3)$$

A constitutive equation known as Darcy's law explains how a nanofluid flows through a porous wedge. The term $Q_0(T_\infty - T)$ is used to calculate the heat source to heat sink ratio for a specific volume., Q_0 is considered to be a constant indicating the amount of heat produced. ($Q_0 > 0$) /absorbed ($Q_0 < 0$) per unit volume. Use the Roseland approximation for thermal radiation. $q''_r = -\frac{4\sigma_1}{3k^*} \frac{\partial T^4}{\partial y}$, σ_1 Stefan-Boltzmann constant, k^* average ratio of absorption.u and v-velocity a component on the x- and y-axes, respectively, T -Base fluid's temperature. β_{hmf} -The thermal expansion coefficient of the hybrid nanofluid, the ρ_{hmf} Density of hybrid nanofluids, k_{hmf} Kinematic viscosity of the hybrid nanofluid, α_{hmf} Heat conduction properties of the hybrid nanofluid.

Thermophysical properties are as follows:

The ternary hybrid nanofluid viscosity model by [35–36].

$$\mu_{Thmf} = \frac{\mu_f}{(1 - \varphi_1)^{2.5} (1 - \varphi_2)^{2.5} (1 - \varphi_3)^{2.5}} \quad (4)$$

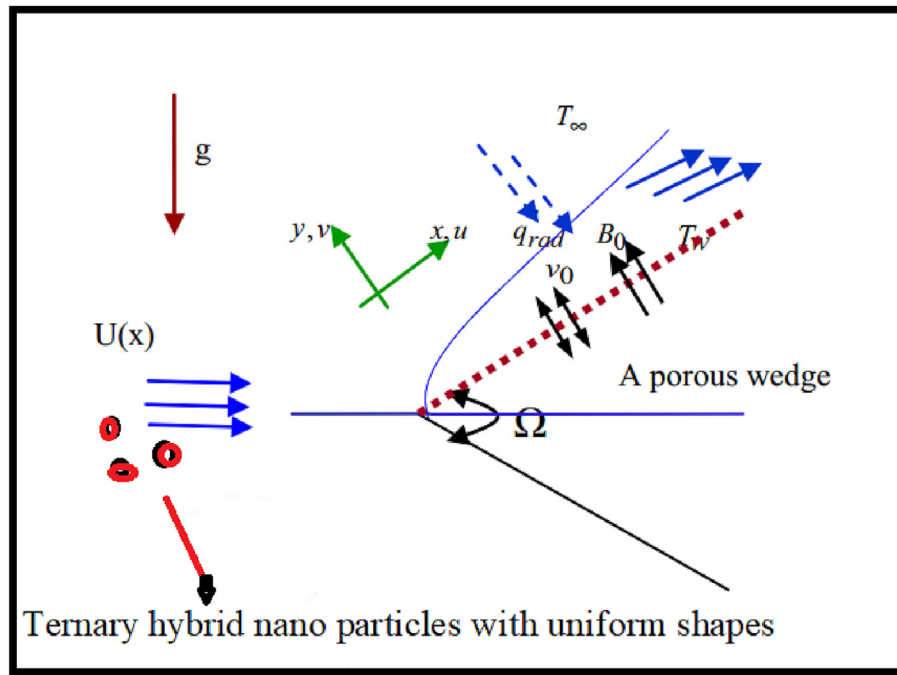


Fig. 1 Flow model porous wedge.

Table 1 Thermophysical properties of Ternary hybrid nanofluid, Nanoparticles with a uniform shape by using the study of [31–32].

	Nomenclature of nano-particles and base fluid	ρ (kg/m ³)	Cp (J/kgK)	K (W/mK)
Base fluid	Polyethylene Glycol-Water	1110	3354	0.3712
Ternary hybrid Nanofluid	AA7072	2720	893	222
	Zirconium oxide	5680	502	1.7
	Magnesium oxide	3560	955	45

The ternary hybrid nanofluid density model by [35–36].

$$\frac{\rho_{Thnf}}{\rho_f} = (1 - \varphi_1) \left\{ (1 - \varphi_2) \left[(1 - \varphi_3) + \frac{\varphi_3 \rho_{sp3}}{\rho_f} \right] + \frac{\varphi_2 \rho_{sp2}}{\rho_f} \right\} + \frac{\varphi_1 \rho_{sp2}}{\rho_f}. \quad (5)$$

The specific heat model for the ternary hybrid nanofluid is as follows: [35–36].

$$\begin{aligned} \frac{(\rho c_p)_{Thnf}}{(\rho c_p)_f} &= \varphi_1 \frac{(\rho c_p)_{sp1}}{(\rho c_p)_f} + (1 - \varphi_1) \\ &\times \left[(1 - \varphi_2) \left\{ (1 - \varphi_3) + \varphi_3 \frac{(\rho c_p)_{sp3}}{(\rho c_p)_f} \right\} + \varphi_2 \frac{(\rho c_p)_{sp2}}{(\rho c_p)_f} \right]. \end{aligned} \quad (6)$$

The ternary hybrid nanofluid thermal conduction model by [35–36].

$$\begin{aligned} \frac{k_{Thnf}}{k_{hf}} &= \frac{(k_3 + 2k_{hf} - 2\varphi_3(k_{hf} - k_3))}{(k_3 + 2k_{hf} + \varphi_3(k_{hf} - k_3))} \\ \frac{k_{hf}}{k_{nf}} &= \frac{(k_2 + 2k_{hf} - 2\varphi_2(k_{hf} - k_2))}{(k_2 + 2k_{hf} + \varphi_2(k_{hf} - k_2))} \\ \frac{k_{nf}}{k_f} &= \frac{(k_1 + 2k_f - 2\varphi_1(k_f - k_1))}{(k_1 + 2k_f + \varphi_1(k_f - k_1))} \end{aligned} \quad (7)$$

The ternary hybrid nanofluid thermal expansion coefficient model by [35–36].

$$\frac{(\rho\beta)_{hf}}{\rho_f} = \frac{(1 - \varphi_1) \left\{ (1 - \varphi_2) \left[(1 - \varphi_3) + \frac{\varphi_3(\rho\beta)_{sp3}}{\rho_f} \right] + \frac{\varphi_2(\rho\beta)_{sp2}}{\rho_f} \right\} + \frac{\varphi_1(\rho\beta)_{sp2}}{\rho_f}}{(1 - \varphi_1) \left\{ (1 - \varphi_2) \left[(1 - \varphi_3) + \frac{\varphi_3 \rho_{sp3}}{\rho_f} \right] + \frac{\varphi_2 \rho_{sp2}}{\rho_f} \right\} + \frac{\varphi_1 \rho_{sp2}}{\rho_f}}. \quad (8)$$

Fluid's kinematic viscosity v_{bf} , φ percentage of hybrid nanoparticles in volume, $(\rho c_p)_{hf}$ Hybrid Nanoparticles' actual thermal capacity, k_{hf} hybrid nano fluid's thermal conductivity, k_{hf} and k_s Basic fluid thermal conductivities and hybrid nanoparticles, ρ_{hf} and ρ_s base fluid and hybrid nanoparticle densities The following are the related boundary conditions:

$$v = 0, u = 0, T = T_w + c_1 x^{n_1} \text{ at } y = 0.$$

$$u \rightarrow U = (v_f x^m) (\delta^{-m-1}) T \rightarrow T_\infty \text{ as } y \rightarrow \infty.$$

c_1 and n_1 (Power Index) are fixed values, and v_0 for the suction ($v_0 > 0$) and for injection ($v_0 < 0$) fluid's flow rate at the wedge. The expression of potential flow velocity is $U(x, t) = \frac{v_f x^m}{\delta^{m+1}}, \beta_1 = \frac{2m}{1+m}$ (see in Sattar [37]) δ time-varying length scale, which is thought to be $\delta = \delta(t)$ and β_1 Typically, the Hartree pressure gradient parameter $\beta_1 = \frac{\Omega}{\Pi}$ for the overall angle Ω within the wedge. By Kifissia and Nanoose's [38], stream function is described as

$$\zeta = y \sqrt{\frac{(1+m)}{2}} \sqrt{\frac{x^{m-1}}{\delta^{m+1}}}, \psi = f(\zeta) \frac{v_f x^{\frac{m+1}{2}}}{\delta^{\frac{m+1}{2}}} \sqrt{\frac{2}{1+m}}, \quad (9)$$

$$\theta = \frac{T - T_\infty}{T_w - T_\infty}, u = \frac{\partial \psi}{\partial y}, \text{ and } v = -\frac{\partial \psi}{\partial x} \quad (10).$$

Equation (2),3 become

$$\begin{aligned} &\left(\frac{\partial^2 \psi}{\partial t \partial y} + \frac{\partial \psi}{\partial y} \frac{\partial^2 \psi}{\partial x \partial y} - \frac{\partial \psi}{\partial x} \frac{\partial^2 \psi}{\partial y^2} \right) \\ &= \frac{1}{A_2} \left[\left\{ A_5 g \Delta T \sin \frac{\Omega}{2} \theta \right\} + \frac{v_{hf}}{A_2} \frac{\partial^3 \psi}{\partial y^3} + U \frac{dU}{dx} - \left(A_1 \frac{\sigma B_0^2}{\rho_{hf}} + \frac{v_{hf}}{K} \right) (u - U) \right] \end{aligned} \quad (11)$$

$$\begin{aligned} &\left(\frac{\partial T}{\partial t} + \frac{\partial T}{\partial x} \frac{\partial \psi}{\partial y} - \frac{\partial T}{\partial y} \frac{\partial \psi}{\partial x} \right) \\ &= \frac{1}{A_4} \left[\frac{1}{Pr} \left\{ A_3 \frac{\partial^2 T}{\partial y^2} + \frac{4}{3} N \left((C_T + T)^3 \theta' \right) \right\} - \frac{Q_o \Delta T}{(\rho c_p)_f} \theta \right] \end{aligned} \quad (12)$$

Boundary conditions.

$$\frac{\partial \psi}{\partial x} = 0, \frac{\partial \psi}{\partial y} = 0, T = T_w \text{ at } y = 0; \quad (13).$$

$$\frac{\partial \psi}{\partial y} \rightarrow \frac{v_m}{\delta^{m+1}}, T \rightarrow T_\infty \text{ as } y \rightarrow \infty \quad (14).$$

$C_T = \frac{T_\infty}{T_w} - T_\infty$ – where the temperature ratio C_T as per its definition, it is based on a very small constant $T_w - T_\infty \gg T_\infty$.

It is given the value in this study $C_T = 0.1$, Murthy et al. [39].

Using traditional Lie group analysis, the Eqs' symmetry groups. (11) and (12) are determined and are defined as

$$x^* = \varepsilon \xi_1(x, y, \psi, \theta) + x, y^* = \varepsilon \xi_2(x, y, \psi, \theta) + y,$$

$$\psi^* = \psi + \varepsilon \mu_1(x, y, \psi, \theta), \theta^* = \theta + \varepsilon \mu_2(x, y, \psi, \theta),$$

It is possible to use algebraic methods to create infinitesimals.

$$\xi_1 = c_2 + c_1 x, \xi_2 = g(x), \mu_1 = c_4 + c_3 \psi \text{ and } \mu_2 = c_5 \theta.$$

$g(x)$ -The infinitesimal generators and arbitrary function are defined as

$$X_3 = \frac{\partial}{\partial \psi} + g(x) \frac{\partial}{\partial y}$$

$$X_1 = \theta \frac{\partial}{\partial \theta} + \psi \frac{\partial}{\partial \psi} + g(x) \frac{\partial}{\partial y} + x \frac{\partial}{\partial x},$$

One-parameter minuscule The specified PDEs are transformed into a system of ODES using Lie group transformation as a specific illustration of Lie group symmetry group transformation.

The defining characteristic equations are

$$\frac{d\theta}{\theta} = \frac{dy}{0} = \frac{dx}{x} = \frac{d\psi}{\psi}$$

We obtain by resolving the equations.

$\psi = x f(\zeta), \zeta = y$, and $\theta = x \theta(\zeta)$ where $\zeta = \zeta(x, t)$. Equations (11), 12 result as follows

$$\begin{aligned} f'' + A_1 A_2 \xi^2 & \left[\lambda_v (\zeta f'' - 2 + 2f') + ff'' + (1 - f^2) \frac{2m}{m+1} \right] + \\ \frac{2}{m+1} & \left[\{(A_1 A_5)\} \times \xi^{\frac{1}{1-m}} \gamma \sin \frac{\Omega}{2} \theta - ((M A_1 + \lambda)(f' - 1)) \right] + \quad (15) \\ (A_2 A_1) \frac{1-m}{1+m} \xi \frac{\partial f}{\partial \xi} & \left(\frac{\partial f}{\partial \xi} - \frac{\partial^2 f}{\partial \xi^2} \right) = 0 \end{aligned}$$

$$\theta'' + \frac{4}{3A_3} N \left\{ (c_T + \theta)^3 \theta' \right\} - \left(\frac{\text{Pr} A_4}{A_3} \right) \left[\frac{\frac{2n_1}{m+1} f \theta + \frac{2}{1+m} \delta_1 \theta - f \theta' + \lambda_v \zeta \theta'}{1+m} \right] = 0 \quad (16)$$

Conditions at the boundaries are as follows.

$$\frac{\partial f}{\partial \xi} = 0, \frac{1-m}{2} \xi \frac{\partial f}{\partial \xi} + \frac{m+1}{2} f = 0, \theta = 1 \text{ at } \zeta = 0 \quad (17).$$

and $\frac{\partial f}{\partial \xi} = 1, \theta \rightarrow 0$ as $\zeta \rightarrow \infty$ (18).

$\text{Pr} = \frac{v_f}{\nu_f}$ is the Prandtl number, $\lambda = \frac{\delta^{m+1}}{Kk^2}$ Porous media parameter, $N = \frac{4\sigma_1 \theta_w^3}{k_{\text{hmf}} k^*}$ thermal radiation parameter, $\theta_w = \frac{1}{T_w - T_\infty} \cdot \gamma = \frac{g(\rho\beta)\Delta T}{\rho_f U^2 k^{1-m}}$ is the natural convection parameter or buoyancy, $\delta_1 = \frac{Q_0 v_f^2}{k_f U^2} \Delta T$ is the parameter for the heat source/sink and $M = \frac{\sigma B_0^2}{\mu_f} \frac{\delta^{m+1}}{k^2}$ the magnetic parameter and $\zeta = \kappa x^{\frac{1-m}{2}}$, By Kifissia and Nanoose's [38] the dimensionless wedge along ($\zeta > 0$). The terms in this system of equations that have partial derivatives with respect to clearly represent the non-similarity aspects of the situation. ξ . This issue forbids similarity-based solutions. Thus, with ξ - In order to solve the system of equations with the derivative terms still present, it is necessary to use a numerical method appropriate for partial differential equations. We will now talk about how to formulate the system of equations for the local similarity model with regard to the current issue. The terms accompanied by are truncated at the first level by $\frac{\partial}{\partial \xi}$ are small. This is especially accurate when ($\xi \ll 1$) .Thus the term with $\xi \frac{\partial}{\partial \xi}$ right-handed side of Eqs. (15) and (16) the following system of equations results after the deletion

$$\begin{aligned} f'' + (D_1 D_2) \left[\lambda_v (-2 + \zeta f'' + 2f') + ff'' + (1 - f^2) \frac{2m}{m+1} \right] + \\ \frac{2}{m+1} \left[\{(D_5 D_1)\} \times \gamma \sin \frac{\Omega}{2} \theta - (D_1 M + \lambda)(f' - 1) \right] = 0 \quad (19) \end{aligned}$$

$$\begin{aligned} \theta'' + \frac{4}{3D_3} N \left\{ (c_T + \theta)^3 \theta' \right\} - \left(\frac{\text{Pr} D_4}{D_3} \right) \left[\frac{2n_1}{m+1} f \theta - f \theta' + \lambda_v \zeta \theta' + \frac{2}{1+m} \delta_1 \theta \right] = 0 \quad (20) \end{aligned}$$

Boundary circumstance are as follows.

$$f = 0, f' = 0, \theta = 1 \text{ at } \zeta = 0 \quad (21).$$

$$\text{and } f' = 1 \theta \rightarrow 0 \text{ as } \zeta \rightarrow \infty \quad (22).$$

Let $\lambda_v = \frac{c}{x^{m-1}}$, where $c = \frac{\delta^m}{v_f} \frac{\partial \delta}{\partial t}$ are integrating,

$\delta = [v_f t c (m+1)]^{\frac{1}{m+1}}$. When $m=1$ and $c=2$ in β_1 , we get $\delta = 2\sqrt{v_f t}$ that acquires the parameter that acquires the parameter δ can be compared to the recognised scaling parameter for problems with unstable boundary layers (see Schlichting [40]). The skin friction coefficient and Nusselt number are defined as

$$c_f = \left(\frac{\partial u}{\partial y} \right)_{y=0} \frac{\mu_{\text{Thnf}}}{\rho_f U^2} = - \frac{\mu_{\text{hmf}}}{\mu_f} (Rex)^{-\frac{1}{2}} f''(0)$$

$$Nu_x = \frac{x k_{\text{hmf}}}{k_f (T_w - T_\infty)} \left(\frac{\partial T}{\partial y} \right)_{y=0}$$

$$= -(Rex)^{\frac{1}{2}} \frac{k_{\text{hmf}}}{k_f} \theta'(0) \left[1 + (c_T + \theta(0))^3 \frac{4}{3} N \right]$$

Reynolds's local number is $Re_x = \frac{U_x}{v_f}$.

Similarity transformations used in Eqs (19) and (20).

$$D_1 = \frac{\rho_{\text{hmf}}}{\rho_f}, D_2 = \frac{\mu_{\text{hmf}}}{\mu_f}, D_3 = \frac{(\rho c_p)_{\text{hmf}}}{(\rho c_p)_f}, D_4 = \frac{k_{\text{hmf}}}{k_{bf}}, D_5 = \frac{(\rho \beta)_{\text{hmf}}}{\rho_f}$$

2.1. Principle of Homogeneity:

$$\frac{\partial v}{\partial y} + \frac{\partial u}{\partial x} = 0 \text{ (Continuity equation)}$$

$$\frac{m}{sm} + \frac{m}{sm} = 0$$

$$\frac{1}{s} + \frac{1}{s} = 0$$

$$\text{(Momentum equation)}$$

$$\begin{aligned} v \frac{\partial u}{\partial y} + u \frac{\partial u}{\partial x} + \frac{\partial u}{\partial t} &= \frac{1}{\rho_{\text{hmf}}} \left[\left(\frac{\partial U}{\partial r} \right) \rho_{\text{hmf}} + \mu_{\text{hmf}} \frac{\partial^2 u}{\partial y^2} + (\rho \beta)_{\text{hmf}} g(T - T_\infty) \sin \frac{\Omega}{2} \right. \\ &\quad \left. - \left(\frac{\sigma B_0^2}{\rho_{\text{hmf}}} \right) (u - U) \right] \end{aligned}$$

$$\frac{m}{s} \frac{m}{sm} + \frac{m}{s} \frac{m}{sm} + \frac{m}{s} \frac{1}{s} = \frac{m}{s} \frac{1}{s} + \frac{m}{s} \frac{m}{sm} + \frac{kgs^{-1} m^{-1}}{kgm^{-3}} \frac{ms^{-1}}{m^2}$$

$$+ \frac{ms^{-1} (kg^{-1} m^{-3} c^2 s) (kg^2 s^{-2} c^{-2})}{kgm^{-3}} + m^2 s^{-1} \frac{m}{s} + \frac{1}{k} (ms^{-2}) k$$

$$\frac{m}{s^2} + \frac{m}{s^2} + \frac{m}{s^2} = \frac{m}{s^2} + \frac{m}{s^2} + \frac{m}{s^2} + \frac{m}{s^2} + \frac{m}{s^2}$$

$$v \frac{\partial T}{\partial y} + u \frac{\partial T}{\partial x} + \frac{\partial T}{\partial t} = \frac{1}{(\rho c_p)_{\text{hmf}}} \left(k_{\text{hmf}} \frac{\partial^2 T}{\partial y^2} - \frac{\partial q_r}{\partial y} - Q_0 (T - T_\infty) \right)$$

$$\text{(Energy equation)}$$

$$\begin{aligned} \frac{ms^{-1} k}{m} + \frac{ms^{-1} k}{m} + \frac{k}{s} &= \frac{k}{s} - \frac{kgm^{-1} s^2 k^{-1}}{m} \left(\frac{kgs^{-3} m^2 m^{-1}}{m} \right) - \frac{kgs^{-4} m^2 k^{-1}}{kgm^{-3} m^2 k^{-1}} \\ \frac{k}{s} + \frac{k}{s} + \frac{k}{s} &= \frac{k}{s} - \frac{k}{s} - \frac{k}{s} \end{aligned}$$

This helps us continue with the further investigation of current study and the all the results are discussed in section 3.

3. Results and interpretation

This work reports heat transfer through a moving porous wedge in the presence of thermal radiation, a heat source or sink, a magnetic field, a Darcy ternary hybrid nanofluid flow, and thermal radiation. To examine the impact of different factors on velocity, simulations are run. $f'(\zeta) = \left(\frac{df}{d\xi} \right)$ velocity and thermal energy $\theta(\zeta)$ fields. Velocity $\frac{df}{d\xi}$ and thermal energy $\theta(\zeta)$ fields is compared for three cases and is portrayed through the construction of graphs Figs. 2 to 19. Here

Case1 Nanofluid (AA7072: Polyethylene Glycol-Water).

Case2 Hybrid nanofluid (AA7072 + Zirconium oxide: Polyethylene Glycol-Water).

Case3 Ternary hybrid nanofluid (AA7072 + Zirconium oxide + Magnesium oxide: Polyethylene Glycol-Water).

The thermophysical properties of base fluid and nanoparticles are listed in Table 1.

Fig. 2 discloses impact of the Magnetic parameter (M) on temperature ($\theta(\zeta)$) profile while other parameters are considered constant. It is evident that $\frac{df}{d\xi}$ of fluid motion is accelerated by the fluid profile along the wedge's wall with an improvement in M Nanofluid, hybrid nanofluid, and ternary hybrid

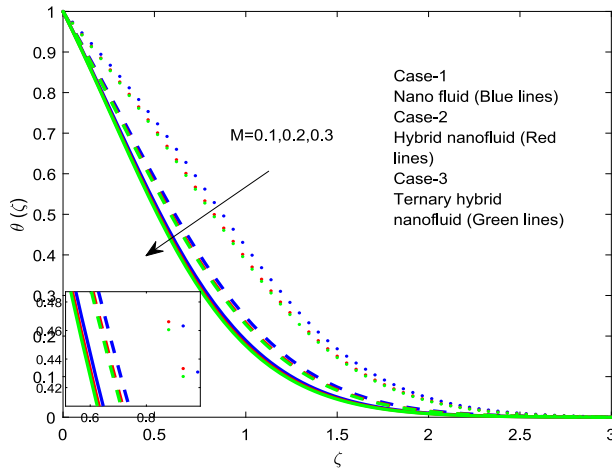


Fig. 2 The impact of M on temperature profile.

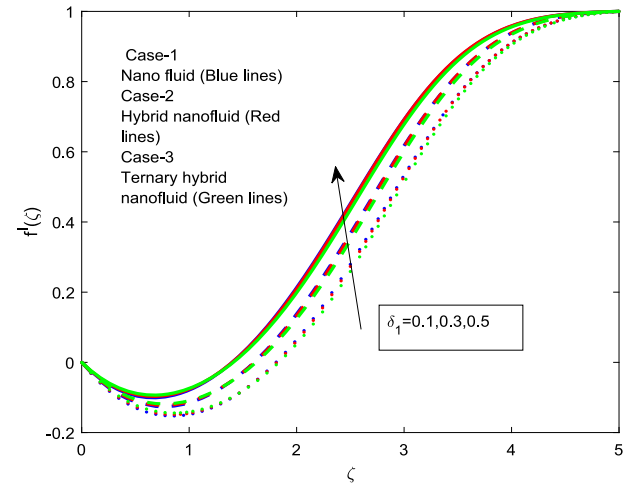


Fig. 4 The impact of δ_1 on velocity profile.

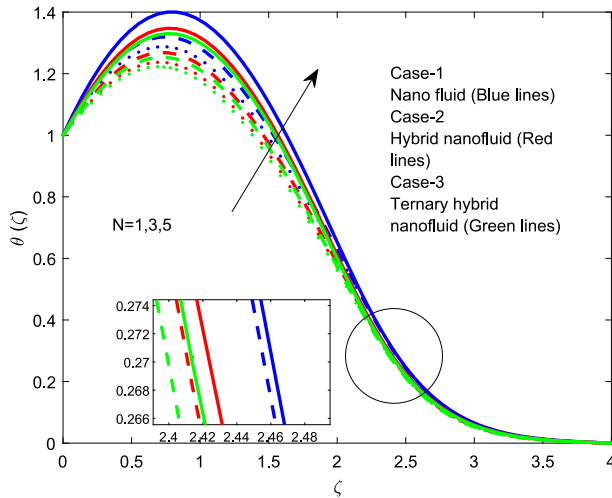


Fig. 3 The impact of N on temperature profile.

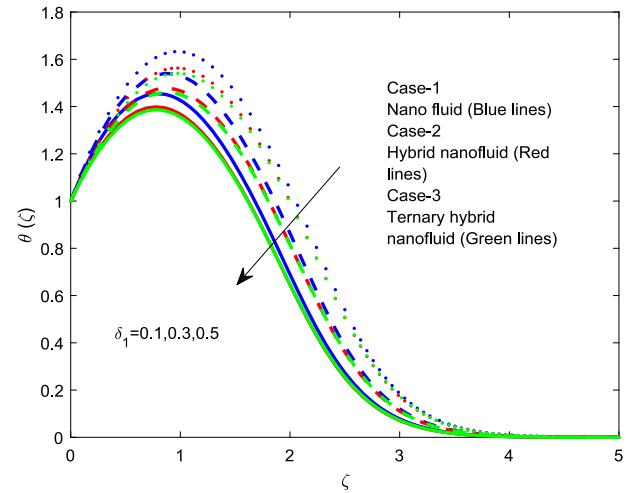


Fig. 5 The impact of δ_1 on temperature profile.

nanofluid are all three examples. In **Fig. 2** $\theta(\zeta)$ profile was increasing for a fluid flow over a Wedge. **Fig. 3** represents the impact of Thermal radiation (N) on $\theta(\zeta)$,The temperature profile was rising while the velocity profile was falling. **Figs. 4 and 5** will represents the impact of Heat source/Sink (δ_1) on $\frac{df}{d\zeta}$ and $\theta(\zeta)$,The temperature profile was falling while the velocity profile was raising. **Fig. 6** will represents the impact of porous parameter (λ) on $\theta(\zeta)$,The temperature profile dropped as the porous layers rises. **Fig. 7** will represents the impact of Buoyancy/Natural convection (γ) on $\theta(\zeta)$,As the temperature profiles rises. The buoyancy generates opposite force on the flow due to this observed in enhancement. **Fig. 8** will represents the impact of m on $\theta(\zeta)$,The temperature profile is rising as m rising due to higher pressure gradient on the system in all the three cases of the flow.

Figs. 9 and 10 will represents the impact of Temperature ratio (C_T) on $\frac{df}{d\zeta}$ and $\theta(\zeta)$,The temperature profile dropped as the velocity profile rise for all the three cases of the flow. As expected temperature ratio improves the internal pressure this help move the particles faster, whereas temperature reduces. **Fig. 11** will signifies the impact of Boundary layer thickness (λ_γ) on $\theta(\zeta)$,While the temperature profiles are having mixed nature in all the three cases of the flow.

Figs. 12 and 19 will represents the impact of Power index parameter (n_1) on $\frac{df}{d\zeta}$ and $\theta(\zeta)$,The temperature profile is rising as the velocity profile is descending.

Table 2 and 3 represents using a different dimension less parameters, will represents the Skin friction and Nusselt number transfer rate. When (M) raises Skn (Skin friction) is decreasing in all the three cases, when we compared three cases

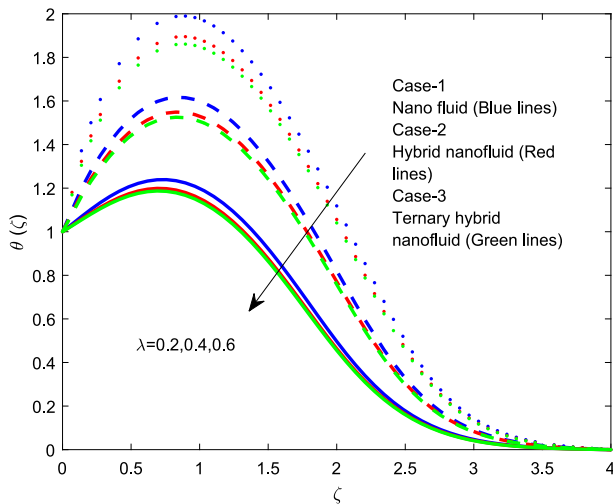


Fig. 6 The impact of λ on temperature profile.

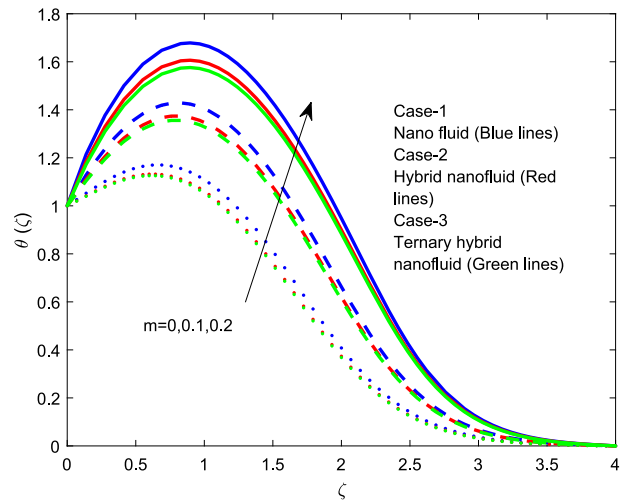


Fig. 8 The impact of m on temperature profile.

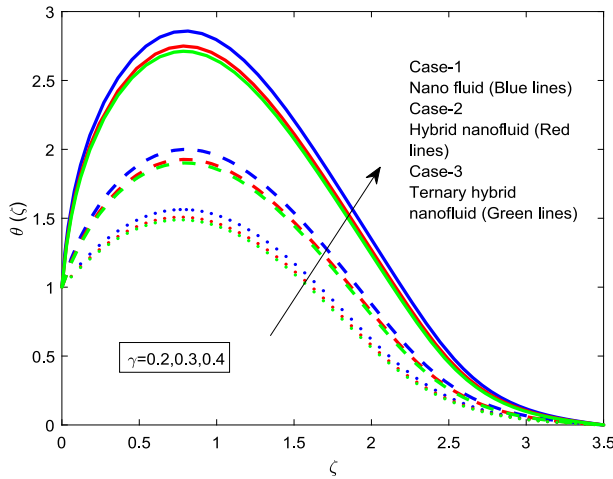


Fig. 7 The impact of γ on temperature profile.

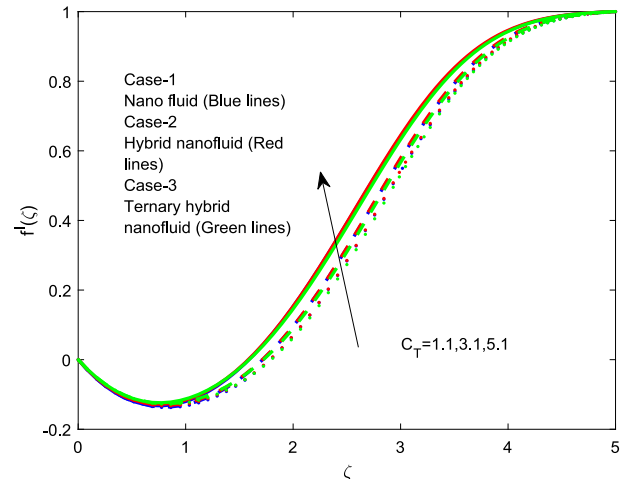


Fig. 9 The impact of C_T on velocity profile.

Case-3 having more Skin friction rate than Case:1&2. When (N) raises Skn (Skin friction) is increasing in all the three cases, when we compared three cases Case-1 having more Skin friction rate than Case:2&3. When λ raises Skn (Skin friction) is increasing in all the three cases, when we compared three cases Case-1 having more Skin friction rate than Case:2&3. When λ_y raises Skn (Skin friction) is increasing in all the three cases, when we compared three cases Case-1 having more Skin friction rate than Case:2&3. **Table 4**.**Table 5**.**Table 6**.

When δ_1 raises Skn (Skin friction) is increasing in all the three cases, when we compared three cases Case-1 having more Skin friction rate than Case:2&3. When n_1 raises Skn (Skin friction) is increasing in all the three cases, when we compared three cases Case-3 having more Skin friction rate than Case:1&2. When m raises Skn (Skin friction) is increasing in all the three cases, when we compared three cases Case-1

having more Skin friction rate than Case:2&3. When C_T raises Skn (Skin friction) is decreasing in all the three cases, when we compared three cases Case-1 having more Skin friction rate than Case:2&3. When γ raises Skn (Skin friction) is decreasing in all the three cases, when we compared three cases Case-1 having more Skin friction rate than Case:2&3. From **Table 3** When M raises Nus (Nusselt number) is decreasing in all the three cases, when we compared three cases Case-2 having more Nusselt number rate than Case:1&3. When N raises Nus (Nusselt number) is decreasing in all the three cases, when we compared three cases Case-1 having more Nusselt number rate than Case:2&3. When λ raises Nus (Nusselt number) is increasing in all the three cases, when we compared three cases Case-1 having more Nusselt number rate than Case:2&3. When λ_y raises Nus (Nusselt number) is increasing in all the three cases, when we compared three cases Case-1 having more Nusselt

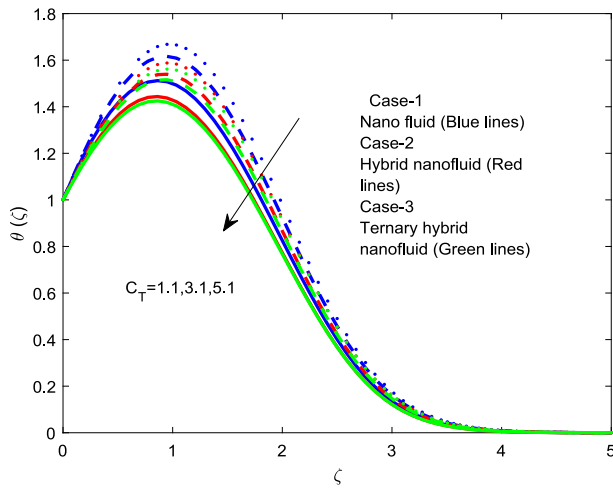


Fig. 10 The impact of C_T on temperature profile.

number rate than Case:2&3. When δ_1 raises Nus (Nusselt number) is increasing in all the three cases, when we compared three cases Case-1 having more Nusselt number rate than Case:2&3. When n_1 raises Nus (Nusselt number) is decreasing in all the three cases, when we compared three cases Case-1 having more Nusselt number rate than Case:2&3. When m raises Nus (Nusselt number) is decreasing in all the three cases, when we compared three cases Case-1 having more Nusselt number rate than Case:2&3. When C_T raises Nus (Nusselt number) is decreasing in all the three cases, when we compared three cases Case-1 having more Nusselt number rate than Case:2&3. When γ raises Nus (Nusselt number) is decreasing in all the three cases, when we compared three cases Case-1 having more Nusselt number rate than Case:2&3.

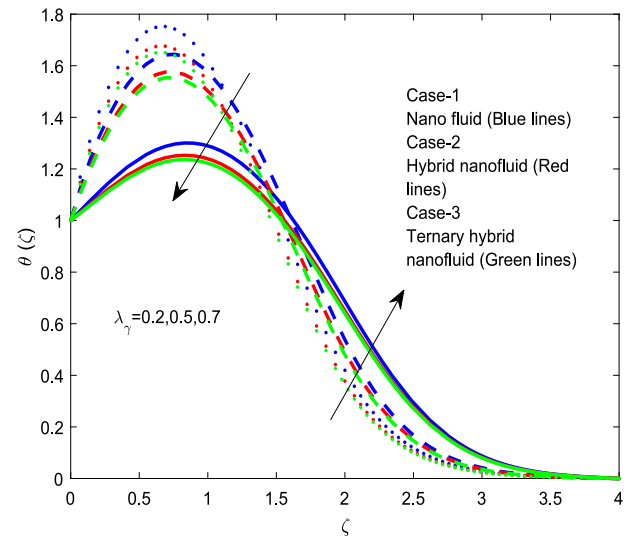


Fig. 11 The impact of λ_γ on temperature profile.

3.1. Multilinear regression analysis:

By using the study of CSK Raju et al. [41], A regression model known as multiple linear regression uses a straight line to evaluate the connection between a quantitative dependent variable and two or more independent variables.

$$\text{i.e., } Z = \beta_0 + \beta_1 * Y_1 + \beta_2 * Y_2 + \beta_3 * Y_3 + \dots$$

Multilinear regression (MLR) analyses the correlation between the different parameters for the resultant solution.

Skin friction for the parameter $\varphi, \varphi_1, \varphi_2, \varphi_3, \lambda_\gamma, \gamma, M$.

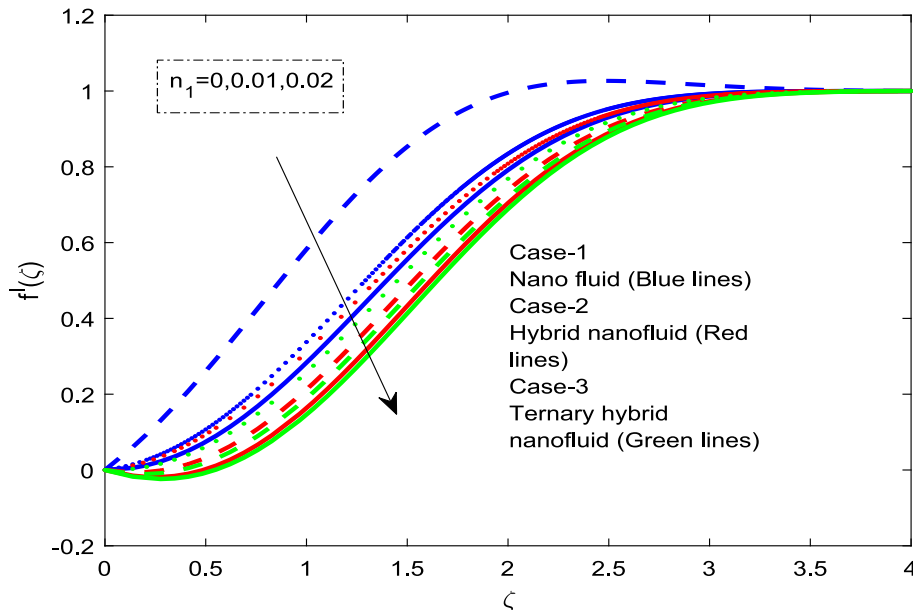
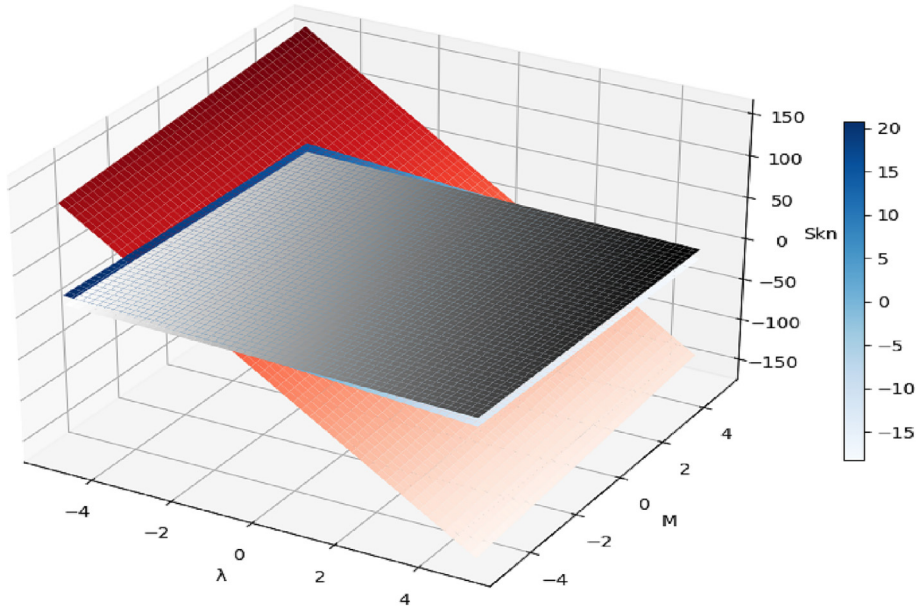
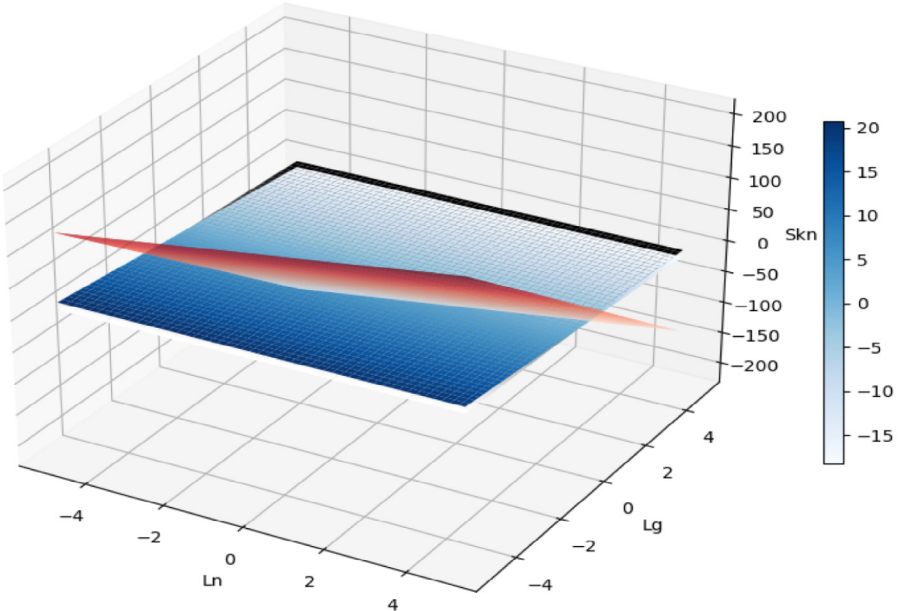
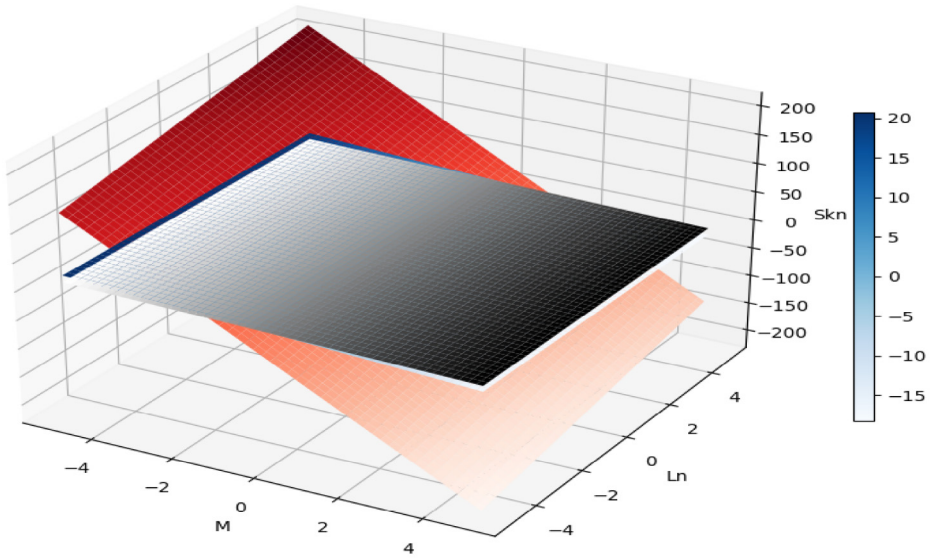
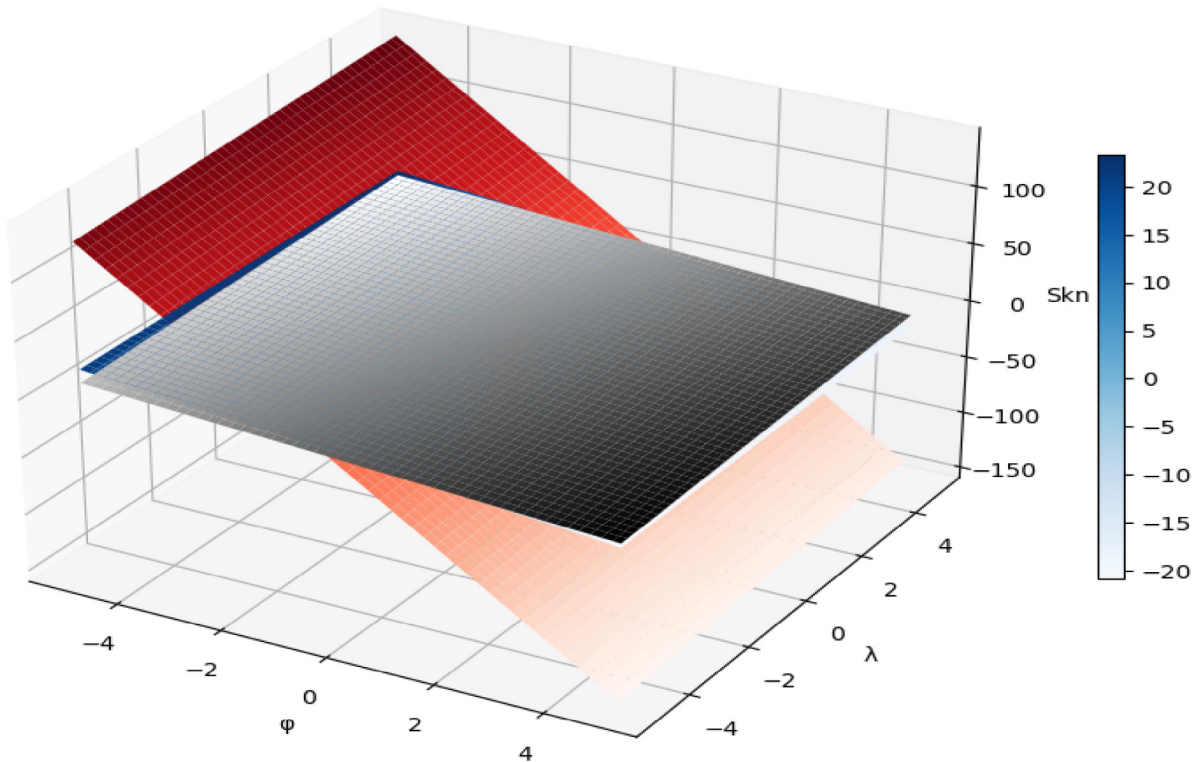


Fig. 12 The impact of n_1 on velocity profile MLR Graphs: Case-1 with red colour, Case-2 with Gray colour, Case-3 with blue colour. (For interpretation of the references to colour in this figure legend, the reader is referred to the web version of this article.)

The impact of λ and M on Sk_n **Fig. 13** M, λ on Sk_n .The impact of λ_γ and λ on Sk_n **Fig. 14** Impact of λ_γ, λ on Sk_n .

The impact of λ_γ and M on SknFig. 15 Impact of λ_γ, M on Skn.The impact of φ and λ on SknFig. 16 Impact of φ, λ on Skn.

The impact of φ and λ_γ on Skn

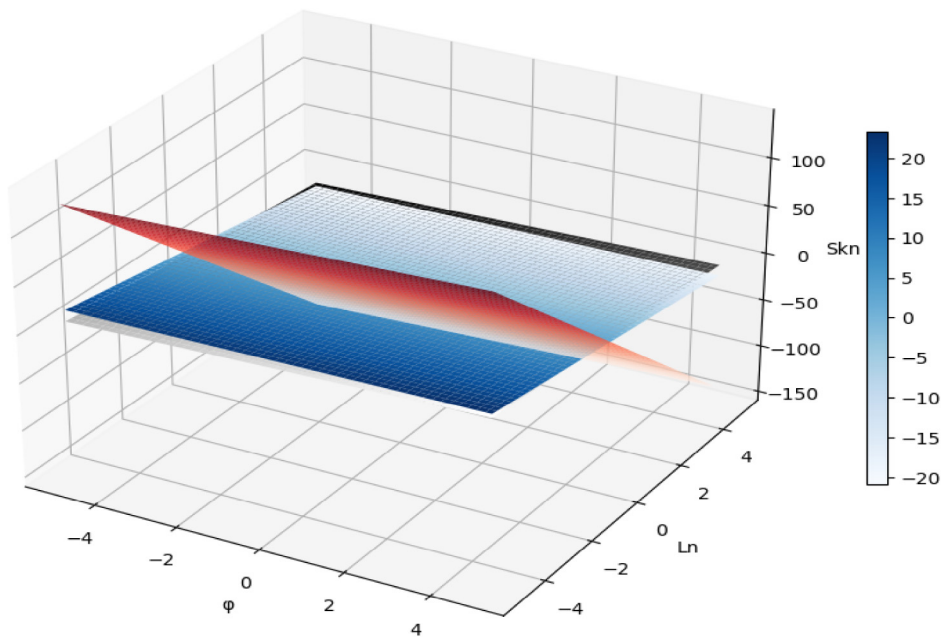


Fig. 17 Impact of φ, λ_γ on Skn .

The impact of φ and M on Skn

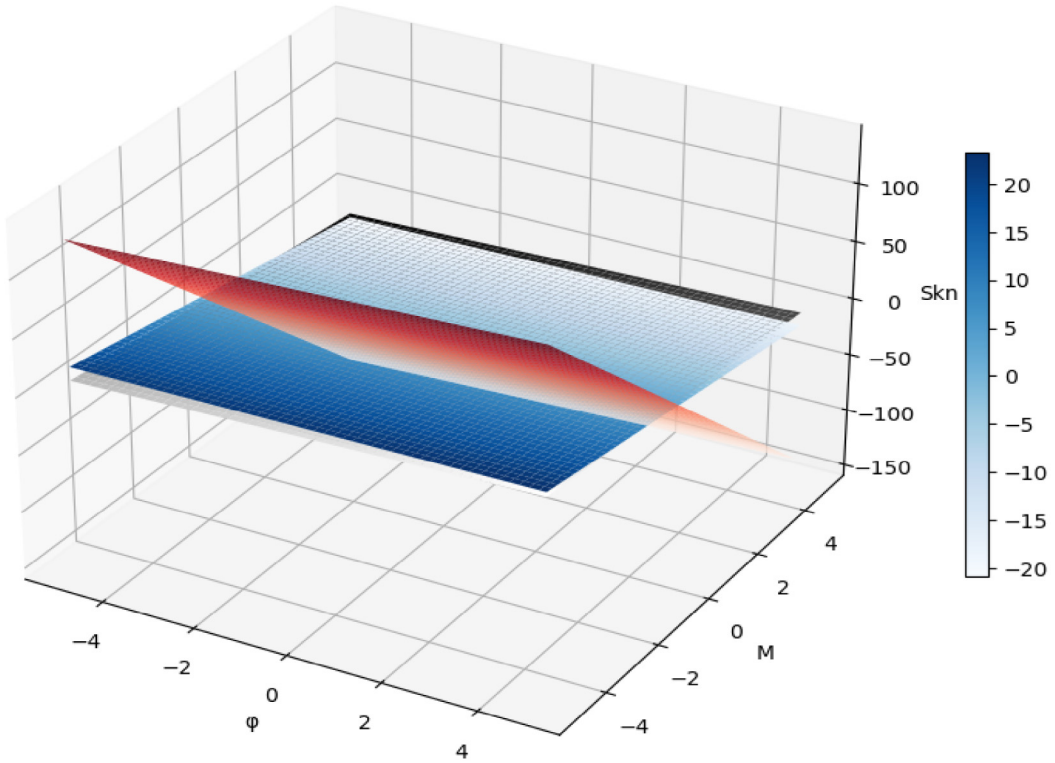


Fig. 18 Impact of M, φ on Skn .

The impact of C_T and δ_1 on Nus

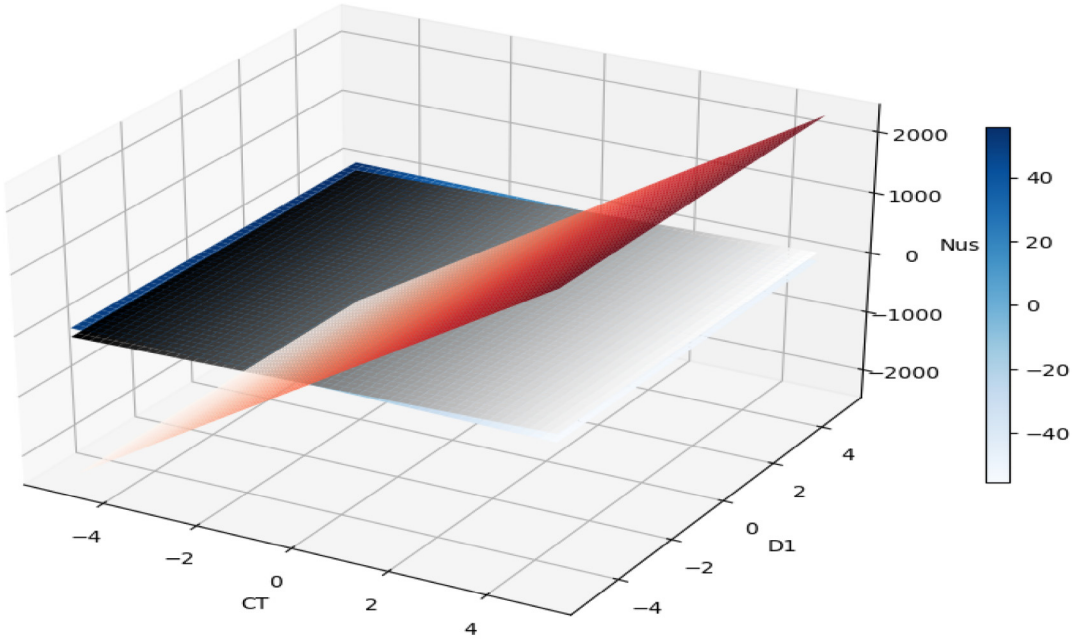


Fig. 19 Impact of C_T, δ_1 on Nus .

Table 2 The physical parameter values for the skin friction coefficient.

M	N	λ	λ_γ	δ_1	n_1	m	C_T	γ	Skin friction		
									Case-1	Case-2	Case-3
0.1									0.276925	0.302120	0.303928
0.2									0.102502	0.133785	0.138419
0.3									0.152924	0.115852	0.103935
	1								0.368026	0.345915	0.326587
	3								0.369517	0.347168	0.327953
	5								0.370666	0.348030	0.328824
	0.2								0.326453	0.304919	0.285883
	0.4								0.361708	0.341576	0.321492
	0.6								0.379699	0.361324	0.341281
	0.2								0.278804	0.256854	0.240482
	0.5								0.549352	0.526050	0.500567
	0.7								0.723548	0.698472	0.667433
	0.2								0.311666	0.291475	0.273136
	0.3								0.347053	0.326119	0.306376
	0.5								0.379250	0.357749	0.337024
	0.1								0.001219	0.140547	0.151985
	0.3								0.390827	0.079160	0.099301
	0.5								0.069121	0.046816	0.014814
	0								0.356916	0.336007	0.317096
	0.01								0.368352	0.346189	0.326780
	0.02								0.363963	0.340544	0.322202
	0								0.360982	0.338698	0.318204
	0.1								0.359674	0.336305	0.315399
	0.2								0.359686	0.335927	0.314894
	1.1								0.485893	0.472804	0.455457
	3.1								0.467615	0.451741	0.433600
	5.1								0.434492	0.414836	0.395802

Table 3 The physical parameter values for the local Nusselt number.

M	N	λ	λ_γ	δ_1	n_1	m	C_T	γ	Nusselt number		
									Case-1	Case-2	Case-3
0.1									0.907888	0.943149	0.981598
0.2									0.793416	0.831977	0.865409
0.3									0.530928	0.580329	0.605897
	1								1.001836	0.848556	0.817154
	3								0.857369	0.699077	0.668218
	5								0.777857	0.620899	0.590477
	0.2								0.715954	0.602065	0.584403
	0.4								2.106886	1.796687	1.735133
	0.6								4.505998	3.780014	3.605518
	0.2								0.555227	0.456246	0.430706
	0.5								1.977464	1.733487	1.691692
	0.7								2.786261	2.443205	2.383802
	0.1								1.244530	1.076671	1.059010
	0.3								1.314884	1.123577	1.089856
	0.5								1.371258	1.154316	1.102158
	0								0.527757	0.525579	0.540261
	0.01								0.567344	0.534721	0.548689
	0.02								0.547407	0.552880	0.562730
	0								1.853137	1.580080	1.498079
	0.1								1.028943	0.880377	0.849208
	0.2								0.383085	0.300532	0.292930
	1.1								1.160093	1.005312	0.976612
	3.1								1.149258	1.016495	0.988483
	5.1								1.137177	1.011060	0.983514
	0.2								15.80462	13.95406	13.639348
	0.3								4.110194	3.662373	3.591247
	0.4								1.609842	1.423502	1.390867

Table 4 Multilinear regression of Skin friction for $\varphi, \varphi_1, \varphi_2, \varphi_3, M, \lambda, \lambda_\gamma$.

Case-1	Coefficients	Standard Error	φ	φ_1	φ_2	φ_3	λ_γ	λ	M	Skn	Probability Percentage
Intercept	-5.57784	0									-5.57784
φ	1.492138	0	0.01	0.01	0	0	0.2	0.2	0.9	0.50722	1.492138
φ_1	-42.1104	0	0.02	0.02	0	0	0.5	0.4	0.6	0.664038	-42.1104
φ_2	0	0	0.03	0.03	0	0	0.7	0.6	0.1	0.819304	0
φ_3	0	0	0.04	0.04	0	0	0.9	0.8	0.2	2.830464	0
λ_γ	8.489935	0	0.05	0.05	0	0	0.6	1	0.3	0.644405	8.489935
λ	2.155894	0	0.009	0.009	0	0	0.2	0.1	1.4	0.279208	2.155894
M	3.045906	0	0.008	0.008	0	0	0.1	1.4	0.7		3.045906
Case-2	Coefficients	Standard Error	φ	φ_1	φ_2	φ_3	λ_γ	λ	M	Skn	Probability Percentage
Intercept	0.962093	0	0.019	0.01	0.009	0	0.2	0.2	0.9	0.496504	0.962093
φ	1.030526	0	0.07	0.02	0.05	0	0.5	0.4	0.6	0.538189	1.030526
φ_1	0	0	0.07	0.03	0.04	0	0.7	0.6	0.1	0.708119	0
φ_2	-1.87223	0	0.07	0.04	0.03	0	0.9	0.8	0.2	0.605985	-1.87223
φ_3	0	0	0.07	0.05	0.02	0	0.6	1	0.3	0.53315	0
λ_γ	0.007356	0	0.019	0.009	0.01	0	0.2	0.1	1.4	0.268185	0.007356
λ	-0.36345	0	0.009	0.008	0.001	0	0.1	1.4	0.7	0.162374	-0.36345
M	-0.48607	0	0.019	0.01	0.009	0	0.2	0.2	0.9	0.496504	-0.48607
Case-3	Coefficients	Standard Error	φ	φ_1	φ_2	φ_3	λ_γ	λ	M	Skn	Probability Percentage
Intercept	1.163712	0	0.069	0.01	0.009	0.05	0.2	0.2	0.9	0.420412	1.163712
φ	0.261267	0	0.1	0.02	0.05	0.03	0.5	0.4	0.6	0.464692	0.261267
φ_1	0	0	0.08	0.03	0.04	0.01	0.7	0.6	0.1	0.676067	0
φ_2	-3.15028	0	0.079	0.04	0.03	0.009	0.9	0.8	0.2	0.54547	-3.15028
φ_3	0	0	0.11	0.05	0.02	0.04	0.6	1	0.3	0.486561	0
λ_γ	-0.12665	0	0.039	0.009	0.01	0.02	0.2	0.1	1.4	0.268208	-0.12665
λ	-0.39342	0	0.049	0.008	0.001	0.004	0.1	1.4	0.7	0.205146	-0.39342
M	-0.57823	0	0.069	0.01	0.009	0.05	0.2	0.2	0.9	0.420412	-0.57823

Table 5 Multilinear regression of Nusselt number for $\varphi, \varphi_1, \varphi_2, \varphi_3, N, C_T, \delta_1$.

Case-1	Coefficients	Standard Error	φ	φ_1	φ_2	φ_3	N	C_T	δ_1	Nus	Probability Percentage
Intercept	-5.57605	0									-5.57605
φ	35.89214	0	0.01	0.01	0	0	0.2	0.2	0.9	16.11139	35.89214
φ_1	441.2306	0	0.02	0.02	0	0	0.5	0.4	0.6	2.644826	441.2306
φ_2	0	0	0.03	0.03	0	0	0.7	0.6	0.1	3.474855	0
φ_3	0	0	0.04	0.04	0	0	0.9	0.8	0.2	10.56416	0
N	1.037022	0	0.05	0.05	0	0	0.6	1	0.3	4.548002	1.037022
C_T	-2.44285	0	0.009	0.009	0	0	0.2	0.1	1.4	0.209796	-2.44285
δ_1	-0.26385	0	0.008	0.008	0	0	0.1	1.4	0.7	1.130892	-0.26385
Case-2	Coefficients	Standard Error	φ	φ_1	φ_2	φ_3	N	C_T	δ_1	Nus	Probability Percentage
Intercept	<i>Coefficients</i>	0	0.019	0.01	0.009	0	0.2	0.2	0.9	15.11986	-0.86988
φ	-0.86988	0	0.07	0.02	0.05	0	0.5	0.4	0.6	1.644674	11.45916
φ_1	11.45916	0	0.07	0.03	0.04	0	0.7	0.6	0.1	2.300181	6.133779
φ_2	6.133779	0	0.07	0.04	0.03	0	0.9	0.8	0.2	1.455225	0
φ_3	0	0	0.07	0.05	0.02	0	0.6	1	0.3	3.16391	0
N	0	0	0.019	0.009	0.01	0	0.2	0.1	1.4	0.201777	0.109368
C_T	0.109368	0	0.009	0.008	0.001	0	0.1	1.4	0.7	1.135358	0.203646
δ_1	0.203646	0	0.019	0.01	0.009	0	0.2	0.2	0.9	15.11986	0.986619
Case-3	Coefficients	Standard Error	φ	φ_1	φ_2	φ_3	N	C_T	δ_1	Nus	Probability Percentage
Intercept	-0.05048	0	0.069	0.01	0.009	0.05	0.2	0.2	0.9	14.4933	-0.05048
φ	14.72721	0	0.1	0.02	0.05	0.03	0.5	0.4	0.6	1.4486	14.72721
φ_1	0	0	0.08	0.03	0.04	0.01	0.7	0.6	0.1	2.19993	0
φ_2	0	0	0.079	0.04	0.03	0.009	0.9	0.8	0.2	1.8844	0
φ_3	-25.5694	0	0.11	0.05	0.02	0.04	0.6	1	0.3	3.02548	-25.5694
N	-0.08292	0	0.039	0.009	0.01	0.02	0.2	0.1	1.4	0.1769	-0.08292
C_T	0.278303	0	0.049	0.008	0.001	0.004	0.1	1.4	0.7	1.19443	0.278303
δ_1	0.718559	0	0.069	0.01	0.009	0.05	0.2	0.2	0.9	14.4933	0.718559

Table 6 The regression statistics for Skin friction and Nusselt number.

Regression Statistics	Skin friction			Nusselt number		
	Case-1	Case-2	Case-3	Case-1	Case-2	Case-3
Multiple R	1	1	1	1	1	1
R Square	1	1	1	1	1	1
Adjusted R Square	65,535	65,535	65,535	65,535	65,535	65,535
Standard Error	0	0	0	0	0	0
Observations	6	6	6	6	6	6

$$\text{Skn}_{\text{case}1} = -5.577 + \varphi * 1.4921 - \varphi_1 * 42.11 + \varphi_2 * 0 + \varphi_3 * 0 + \lambda_\gamma * 8.4899 + \gamma * 2.1558 + M * 3.0459$$

$$\text{Skn}_{\text{case}2} = 0.962 + 1.0305 * \varphi + 0 * \varphi_1 - 1.872 * \varphi_2 + 0 * \varphi_3 + \lambda_\gamma * 0.0073 - 0.363 * \gamma - 0.486 * M \quad (23)$$

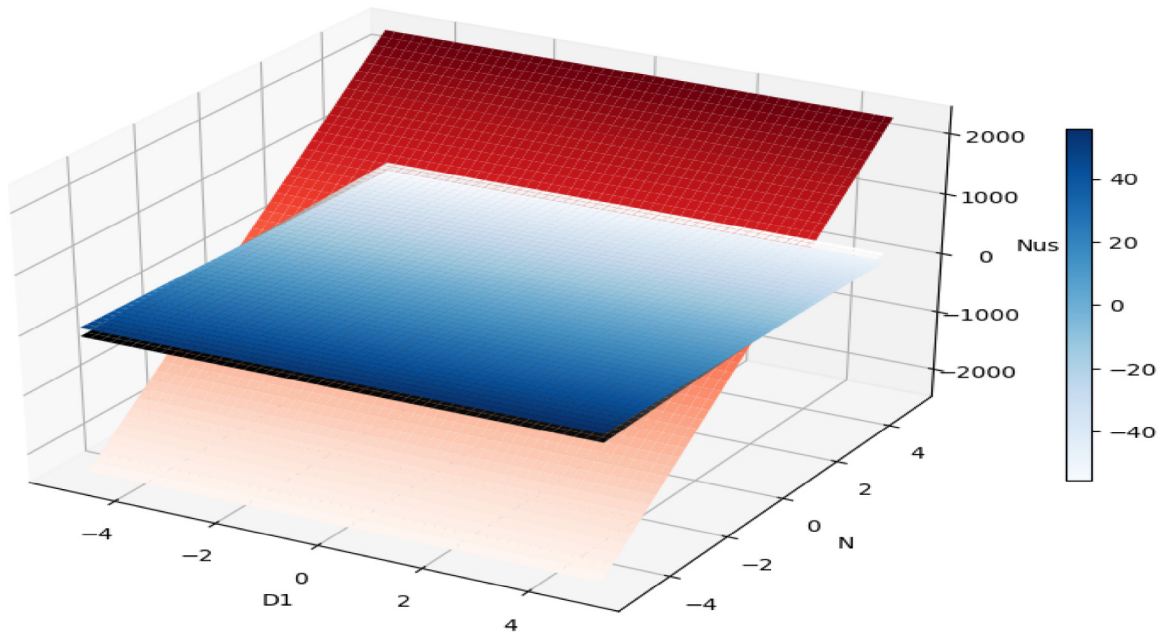
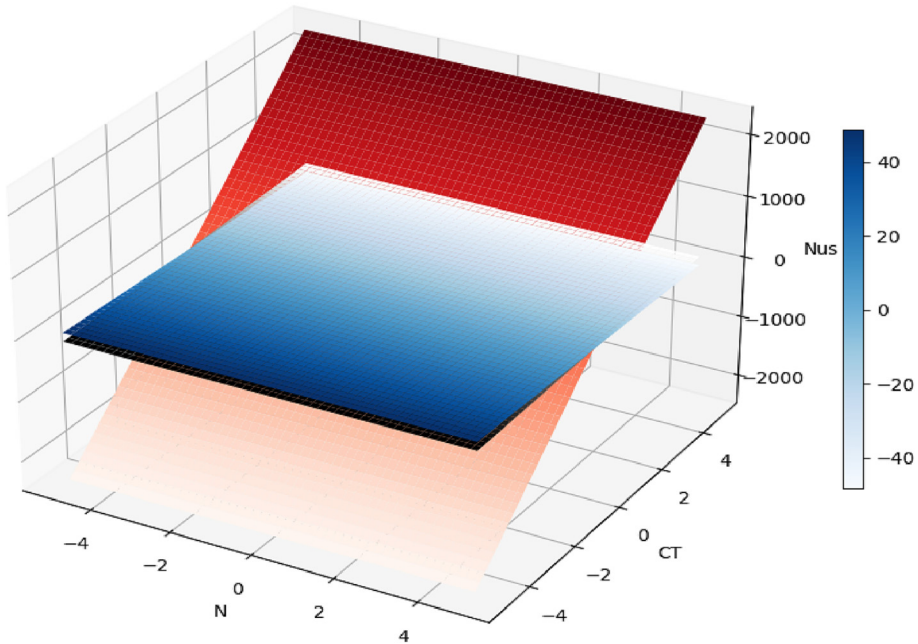
$$\text{Skn}_{\text{case}3} = 1.1637 + \varphi * 0.2612 + 0 * \varphi_1 - 3.1502 * \varphi_2 + \varphi_3 * 0 - 0.1266 * \lambda_\gamma - 0.3934 * \gamma - 0.578 * M$$

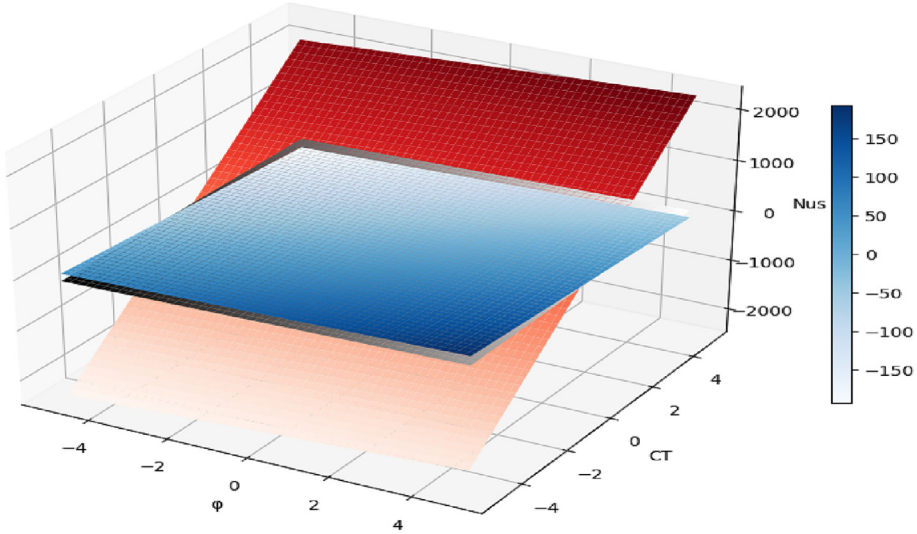
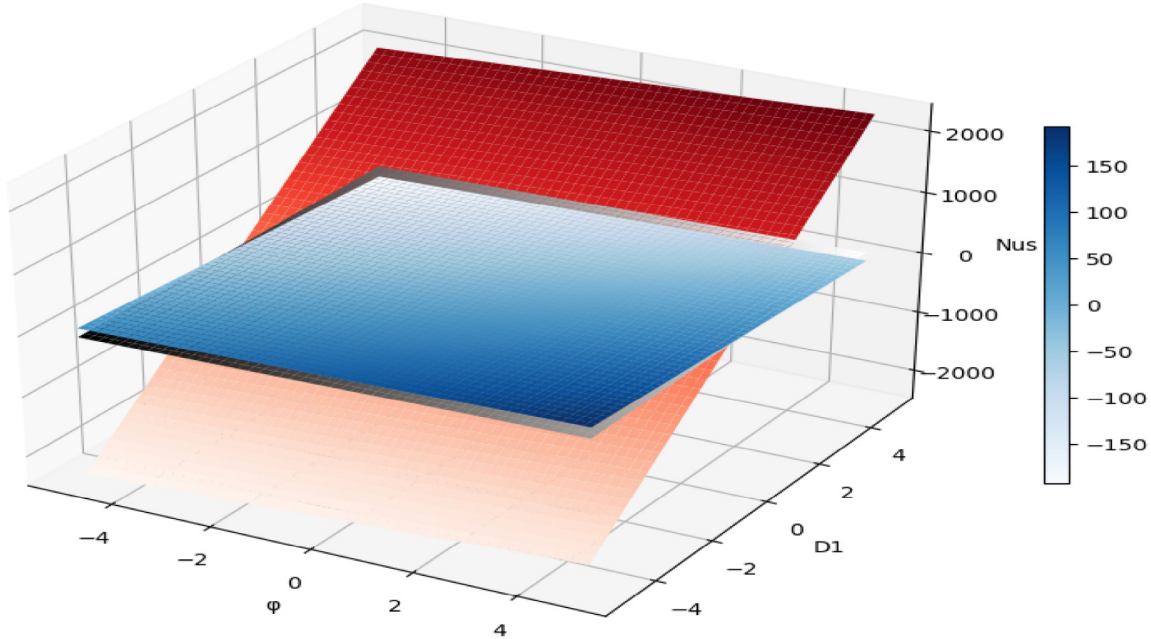
Nusselt number for the parameters $\varphi, \varphi_1, \varphi_2, \varphi_3, N, C_T, \delta_1$.

$$\text{Nus}_{\text{case}1} = -5.576 + 35.892 * \varphi + \varphi_1 * 441.23 + \varphi_2 * 0 + \varphi_3 * 0 + N * 1.037 - 2.442 * C_T - 0.263 * \delta_1$$

$$\text{Nus}_{\text{case}2} = -0.869 + \varphi * 11.4591 + \varphi_1 * 6.1337 + \varphi_2 * 0 + \varphi_3 * 0 + 0.1093 * N + 0.2036 * C_T + 0.9866 * \delta_1 \quad (24)$$

$$\text{Nus}_{\text{case}3} = 0.05 + \varphi * 14.7272 + 0 * \varphi_1 + 0 * \varphi_2 - 25.5694 * \varphi_3 - 0.082 * N + 0.2783 * C_T + 0.718559 * \delta_1$$

The impact of δ_1 and N on Nus**Fig. 20** Impact of N, δ_1 on Nus .**The impact of N and CT on Nus****Fig. 21** Impact of N, C_T on Nus .

The impact of φ and C_T on NusFig. 22 Impact of φ, C_T on Nus.The impact of φ and δ_1 on NusFig. 23 Impact of φ, δ_1 on Nus.

Case-1 with red colour, Case-2 with Gray colour, Case-3 with blue colour.

From Figs. 13-31 with represents the impact of independent parameters on dependent parameter as follows from Fig. 13 we can observe that the impact of M, λ on Skn , Case 2 has a higher rate of skin friction transfer than Cases 1 and 3. Fig. 14 we can observe that the impact of λ_γ, λ on Skn , Case

1 has a higher rate of skin friction transfer than Cases 2 and 3. Fig. 15 we can observe that the impact of λ_γ, M on Skn , Case 2 has a higher rate of skin friction transfer than Cases 1 and 3. Fig. 16 we can observe that the impact of φ, λ on Skn , Case 2 has a higher rate of skin friction transfer than Cases 1 and 3. Fig. 17 we can observe that the impact of φ, λ_γ on Skn , When compared to Cases 1 and 3, Case 2 had a higher rate of skin

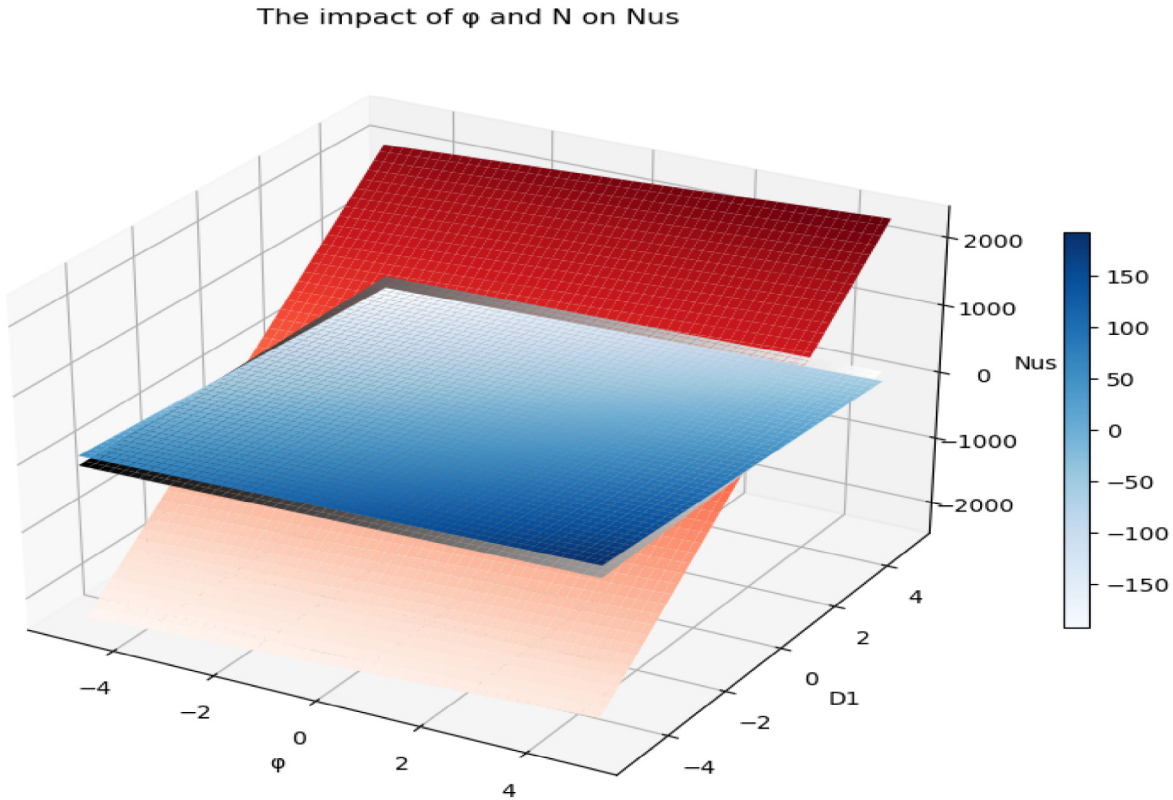


Fig. 24 Impact of φ, N on.

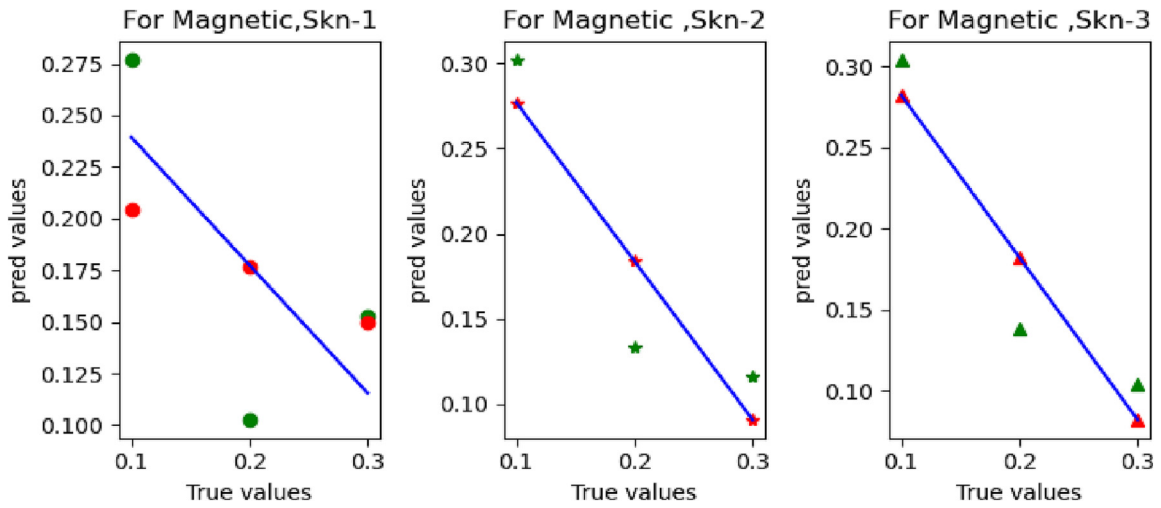


Fig. 25 Magnetic vs Skin friction coefficient.

friction transmission. [Fig. 18](#) we can observe that the impact of M, φ on Skn , Skin friction transfer rate in Case-2 is higher than Cases 1 and 3.

[Fig. 19](#) we can observe that the impact of C_T, δ_1 on Nus , having a higher Nusselt number transfer rate than Cases 1 and 3, Case-2 has more dominance. [Fig. 20](#) we can observe that the impact of N, δ_1 on Nus having a higher Nusselt number transfer rate than Cases 1 and 2, Case 3 has more domi-

nance. [Fig. 21](#) we can observe that the impact of N, C_T on Nus , having a higher Nusselt number transfer rate than Cases 1 and 2, Case 3 has more dominance. [Fig. 22](#) we can observe that the impact of φ, C_T on Nus , Case-3 has a higher rate of Nusselt number transfer than Cases 1 and 2. [Fig. 23](#) we can observe that the impact of φ, δ_1 on Nus , having a higher Nusselt number transfer rate than Cases 1 and 2, Case 3 has more dominance. [Fig. 24](#) we can observe that the impact of φ, N on

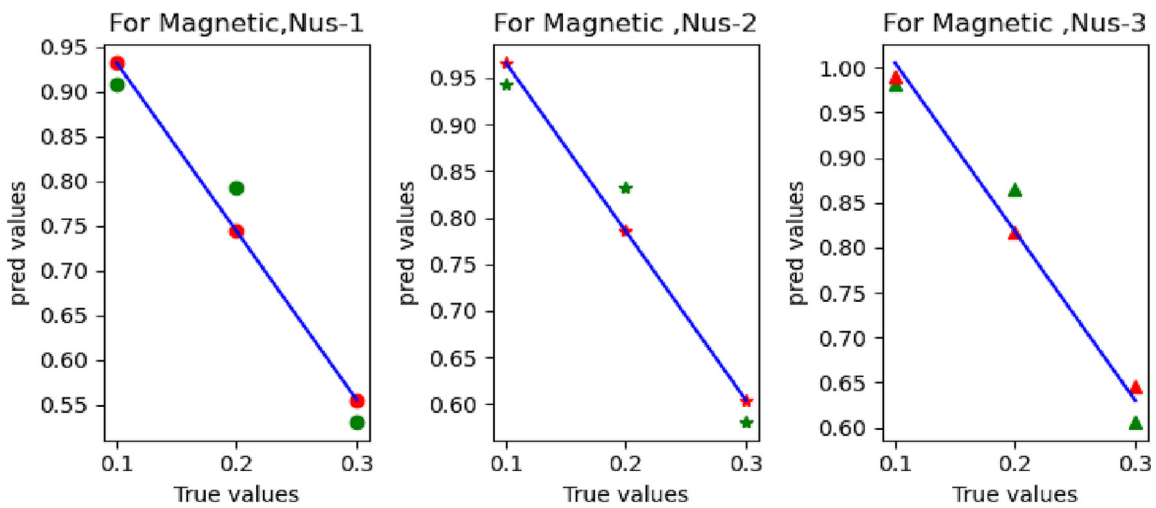


Fig. 26 Magnetic vs Nusselt number.

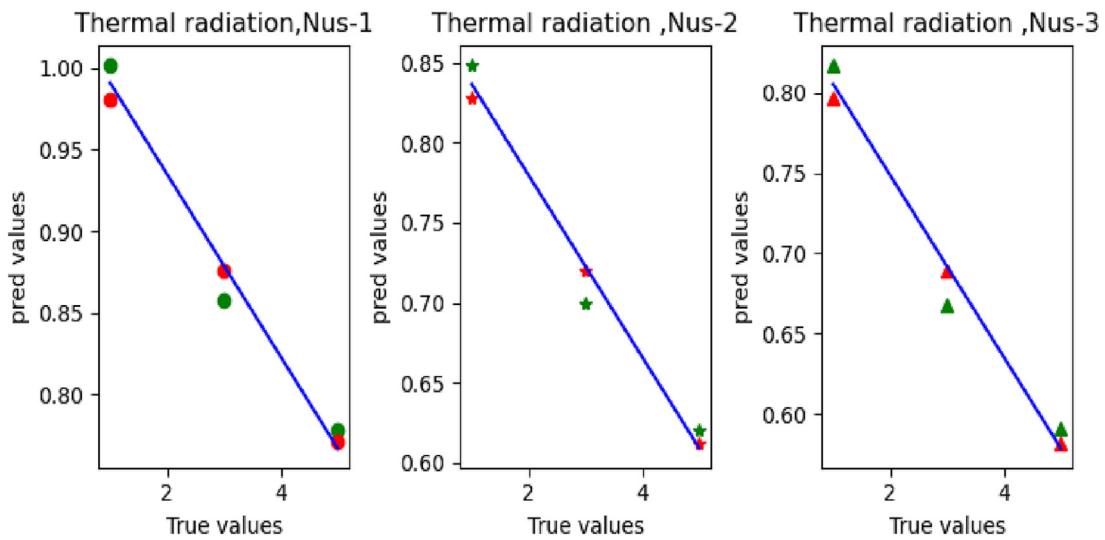


Fig. 27 Thermal radiation vs Nusselt number.

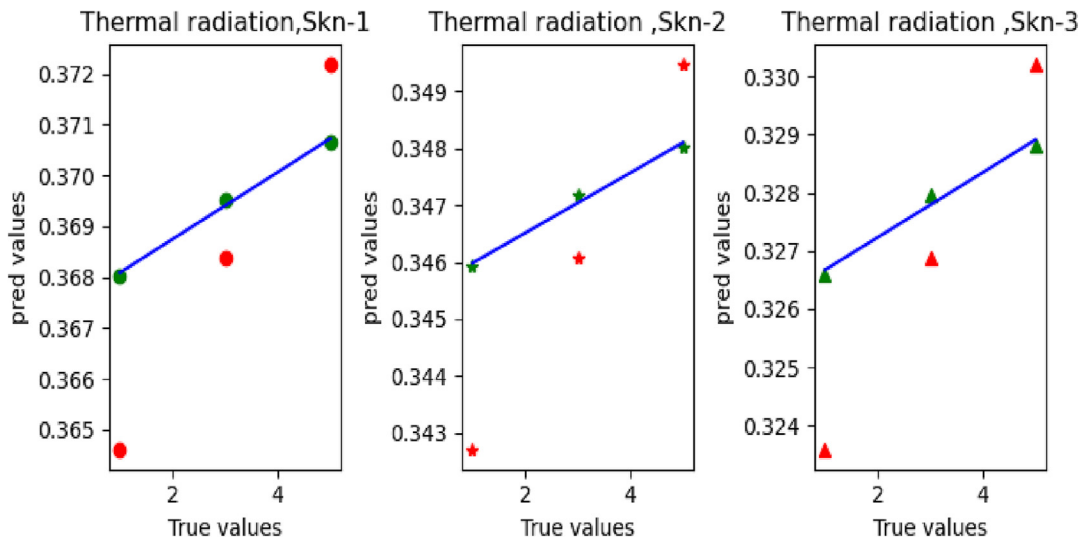
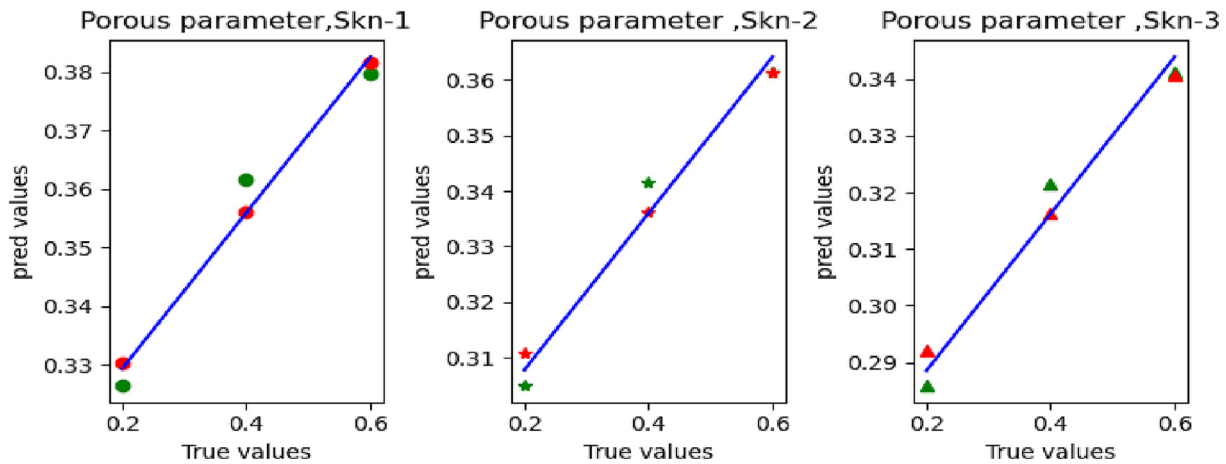
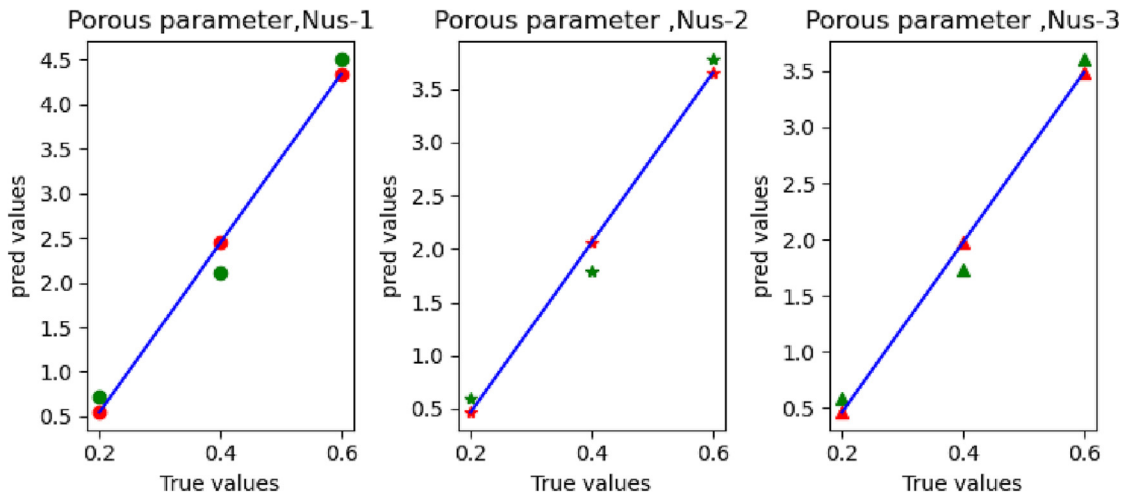


Fig. 28 Thermal radiation vs skin friction coefficient.

**Fig. 29** Porous vs skin friction coefficient.**Fig. 30** Porous vs Nusselt number.**Table 7** Gradient descent Machine learning values for the skin friction coefficient.

M	N	λ	Skn-1		Skn-2		Skn-3	
			True values	Predicted values	True values	Predicted values	True values	Predicted values
0.1			0.276925	0.20453875	0.302120	0.277053	0.303928	0.282090
0.2			0.102502	0.1770057	0.133785	0.183919	0.138419	0.182094
0.3			0.152924	0.14947265	0.115852	0.090785	0.103935	0.0820975
	1		0.368026	0.36459932	0.345915	0.34270458	0.326587	0.32357745
	3		0.369517	0.3683922	0.347168	0.34608725	0.327953	0.32689083
	5		0.370666	0.37218508	0.348030	0.34946992	0.328824	0.33020422
	0.2		0.326453	0.33037313	0.304919	0.310752	0.285883	0.292118
	0.4		0.361708	0.35600005	0.341576	0.33607474	0.321492	0.31637988
	0.6		0.379699	0.38162698	0.361324	0.36139748	0.341281	0.34064176

Table 8 Gradient descent Machine learning values for the local Nusselt number.

M	N	λ	Nus-1		Nus-2		Nus-3	
			True values	Predicted values	True values	Predicted values	True values	Predicted values
0.1			0.907888	0.93255733	0.943149	0.96656167	0.981598	0.98960793
0.2			0.793416	0.74407733	0.831977	0.78515167	0.865409	0.81743246
0.3			0.530928	0.55559733	0.580329	0.60374167	0.605897	0.64525699
	1		1.001836	0.98093928	0.848556	0.8280546	0.817154	0.79697094
	3		0.857369	0.87609857	0.699077	0.72034351	0.668218	0.6895364
	5		0.777857	0.77125787	0.620899	0.61263237	0.590477	0.58210186
		0.2	0.715954	0.547924	0.602065	0.47061417	0.584403	0.4644605
		0.4	2.106886	2.442946	1.796687	2.05958867	1.735133	1.975018
		0.6	4.505998	4.337968	3.780014	3.64856317	3.605518	3.4855755

Table 9 Comparison of study the validity and reliability as follows.

	Kandasamy et al. [33] and Kandasamy et al. [34]	Present results
$M = 0$	0.5911	0.5912
$M = 0.5$	0.6679	0.6680
$M = 1$	0.7504	0.7503

Nus ,Compared to Cases 1 and 2, Case 3 has a higher Nusselt number transfer rate.

3.2. Results of Machine learning analysis for Skin friction and Nusselt. number:

By using Gradient descent method along with simple linear regression analysis, we can see the Figs. 25–30. elucidates comparison of testing versus training skin friction and Nusselt number for (a) Nanofluid case (b) Hybrid nanofluid case (c) Ternary hybrid nanofluid case for Porous, Thermal and Magnetic parameter. The testing data points (red colour) and training data points (green colour) are along the diagonal line. The anticipated values are close to the numerical values as well. Thus, the machine learning algorithms can accurately forecast physical quantities, we see those resultant comparison of True and Predicted values from the Tables 7 and 8.

4. Concluding remarks

The numerical investigation of nanofluid flow and heat transfer properties over a porous wedge includes nanofluid (AA7072: Polyethylene Glycol-Water), hybrid nanofluid (AA7072 + Zirconium oxide: Polyethylene Glycol-Water), and ternary hybrid nanofluid (AA7072 + Zirconium oxide + Magnesium oxide: Polyethylene Glycol-Water). Scaling group transformations were utilised to change dimensional equations into non-dimensional equations. In terms of the operational parameters, machine learning using the gradient

descent approach has been employed to create and optimise a thorough quadratic model for the rate of heat transfer.

The study's main findings are as follows:

- It is found that the Nusselt number transfer rate is more in Ternary hybrid nanofluids than Hybrid and Nanofluids and the Skin friction rate is more in Hybrid nanofluids than in Ternary and Nanofluids
- Heat source/sink, power index and temperature ratio improvements for these parameters the profiles of velocity are increasing.
- Increased Boundary layer thickness having the mixed-nature temperature profiles.
- Temperature profiles are deteriorating as the parameters for magnetic, heat source/sink, porous materials, and temperature ratio are improved.
- The temperature profile is rising due to improvements in the Power index, Hall effect, buoyancy, and thermal radiation parameters.
- The fitted MLR for the Nusselt number is accurate with $R^2 = 1$ in all the three cases.
- By using Gradient descent method with Machine learning approach getting accurate predicted values for Truth values.

Declaration of Competing Interest

The authors declare that they have no known competing financial interests or personal relationships that could have appeared to influence the work reported in this paper.

References

- [1] R. Abdul-Kahar, R. Kandasamy, Lie scaling group transformation for boundary-layer flow of a nanofluid past a porous vertical stretching surface in the presence of chemical reaction with heat radiation, Comput. Fluids 52 (2011) 15–21.
- [2] R. Kandasamy, T. Hayat, S. Obaidat, Group theory transformation for Soret and Dufour effects on free convective heat and mass transfer with thermophoresis and chemical reaction over a porous stretching surface in the presence of heat source/sink, Nucl. Eng. Des. 241 (6) (2011) 2155–2161.

- [3] C.S.K. Raju, N.A. Ameer, K. Sajjan, N.A. Shah, S.-J. Yook, M. K. Dinesh, Nonlinear movements of axisymmetric ternary hybrid nanofluids in a thermally radiated expanding or contracting permeable Darcy Walls with different shapes and densities: Simple linear regression, *Int. Commun. Heat Mass Transf.* 135 (2022) 106110.
- [4] R. Saidur, K.Y. Leong, H.A. Mohammed, A review on applications and challenges of nanofluids, *Renew. Sustain. Energy Rev.* 15 (3) (2011) 1646–1668.
- [5] N.A. Shah, A. Ebaid, T. Oreyeni, S.-J. Yook, MHD and Porous Effects on Free Convection Flow of Viscous Fluid between Vertical Parallel Plates: Advance Thermal Analysis, *Waves Random Complex Media* (2023), <https://doi.org/10.1080/17455030.2023.2186717>.
- [6] R. Abdul-Kahar, R. Kandasamy, I am scaling group transformation for boundary-layer flow of a nanofluid past a porous vertical stretching surface in the presence of chemical reaction with heat radiation, *Comput. Fluids* 52 (2011) 15–21.
- [7] Y. Lin, L. Zheng, X. Zhang, Radiation affects Marangoni convection flow and heat transfer in pseudo-plastic non-Newtonian nanofluids with variable thermal conductivity, *Int. J. Heat Mass Transf.* 77 (2014) 708–716.
- [8] B. Ahmad, A. Nawaz, K. Smida, S.U. Khan, M.I. Khan, T. Abbas, Y.D. Reddy, K. Guedry, M.Y. Malik, B.S. Goud, A.M. Galal, Thermal diffusion of Maxwell nanoparticles with various flow features: Lie group simulations, *Int. Commun. Heat Mass Transfer* 136 (2022) 106164.
- [9] H.A. Ogunseye, Y.O. Tijani, P. Sibanda, Entropy generation in an unsteady Eyring-Powell hybrid nanofluid flow over a permeable surface: A Lie group analysis, *Heat Transfer* 49 (6) (2020) 3374–3390.
- [10] S.U. Mamatha, R.R. Devi, N.A. Ahammad, N.A. Shah, B.M. Rao, C.S.K. Raju, M.I. Khan, K. Guedry, Multi-linear regression of triple diffusive convectively heated boundary layer flow with suction and injection: Lie group transformations, *International Journal of Modern Physics B* 37 (01) (2023) 2350007.
- [11] P. Sreenivasulu, S.R. Gunakala, T. Poornima, N.B. Reddy, V. M. Job, Aligned magnetic field and Navier slip effects on the free convective radiative flow of nanofluids with embedded carbon nanotubes: a Lie group analysis, *SN Applied Sciences* 2 (7) (2020) 1–12.
- [12] M. Biglarian, M.R. Gorji, O. Pourmehran, G. Domairry, H₂O-based different nanofluids with unsteady condition and an external magnetic field on permeable channel heat transfer, *Int. J. Hydrogen Energy* 42 (34) (2017) 22005–22014.
- [13] H. Maleki, M.R. Safaei, A.A. Alrashed, A. Kasaeian, Flow and heat transfer in non-Newtonian nanofluids over porous surfaces, *J. Therm. Anal. Calorim.* 135 (3) (2019) 1655–1666.
- [14] M.J. Uddin, A. Sohail, O.A. Bég, A.M. Ismail, Numerical solution of MHD slip flow of a nanofluid past a radiating plate with Newtonian heating: A Lie group approach, *Alex. Eng. J.* 57 (4) (2018) 2455–2464.
- [15] U.S. Mahabaleshwar, T. Anusha, O.A. Bég, D. Yadav, T. Botmart, Impact of Navier's slip and chemical reaction on the hydromagnetic hybrid nanofluid flow and mass transfer due to porous stretching sheet, *Sci. Rep.* 12 (1) (2022) 1–14.
- [16] M. Hafeez, S. Rehman, M. Oreijah, K. Guedry, O.T. Bafakeeh, A study on dual solutions for water-based hybrid nanofluids flowing through a convergent channel with dissipative heat transport, *J. Indian Chem. Soc.* 99 (11) (2022) 100758.
- [17] S. Ahmad, R. Diyar, S. Zeb, Lie group analysis of hyperbolic tangent fluid flow in the presence of thermal radiation, *Heat Transfer* 51 (4) (2022) 3067–3081.
- [18] I. Waini, A. Ishak, I. Pop, Transpiration effects on hybrid nanofluid flow and heat transfer over a stretching/shrinking sheet with uniform shear flow, *Alex. Eng. J.* 59 (1) (2020) 91–99.
- [19] S. Kavya, V. Nagendramma, N.A. Ahammad, S. Ahmad, C. Raju, N.A. Shah, Magnetic-hybrid nanoparticles with stretching/shrinking cylinder in a suspension of MoS₄ and copper nanoparticles, *Int. Commun. Heat Mass Transfer* 136 (2022) 106150.
- [20] A. Bhattacharyya, R. Sharma, S.M. Hussain, A.J. Chamkha, E. Mamatha, A numerical and statistical approach to capture the flow characteristics of Maxwell hybrid nanofluid containing copper and graphene nanoparticles, *Chin. J. Phys.* 77 (2022) 1278–1290.
- [21] W.K. Usafzai, Multiple exact solutions of second degree nanofluid slip flow and heat transport in porous medium, *Thermal Science and Engineering Progress* 40 (2023) 101759.
- [22] W. Khan Usafzai, R.U. Haq, E.H. Aly, Wall laminar nanofluid jet flow and heat transfer, *Int. J. Numer. Meth. Heat Fluid Flow* (2022).
- [23] W.K. Usafzai, E.H. Aly, Multiple exact solutions for micropolar slip flow and heat transfer of a bidirectional moving plate, *Thermal Science and Engineering Progress* 37 (2023) 101584.
- [24] W.K. Usafzai, E.H. Aly, Exact multiple solutions of 2-D bidirectional moving plate micropolar hybrid nanofluid flow with heat transfer, *Chin. J. Phys.* 80 (2022) 414–426.
- [25] W.K. Usafzai, E.H. Aly, A.S. Alshomrani, M.Z. Ullah, Multiple solutions for nanofluids flow and heat transfer in porous medium with velocity slip and temperature jump, *Int. Commun. Heat Mass Transfer* 131 (2022) 105831.
- [26] S. Nasir, S. Sirisubtawee, N. Akkurt, I. Ali, T. Gul, P. Juntharee, Simultaneous features of ternary hybrid nanoparticles on thermal radiative flow configured by Darcy-Forchheimer porous surface, *Int. J. Mod. Phys. B* (2023) 2450015.
- [27] Saeed, A., Alyami, M.A., Akkurt, N., Khan, T.S. and Gul, T., Ternary hybrid nanofluids flow on a spinning disk with nonlinear thermal radiation. *ZAMM-Journal of Applied Mathematics and Mechanics/Zeitschrift für Angewandte Mathematik und Mechanik*, p.e202200203.
- [28] S. Nasir, S. Sirisubtawee, T. Gul, P. Juntharee, W. Alghamdi, I. Ali, Thermal Characteristics of Nonlinear Convection and Radiation for the Flow of Tri-Hybrid Nanofluids Over Stretchable Surface with Energy Source, *Surf. Rev. Lett.* 29 (11) (2022) 2250153.
- [29] M. Marin, R. Ellahi, S. Vlase, M.M. Bhatti, On the decay of exponential type for the solutions in a dipolar elastic body, *Journal of Taibah University for Science* 14 (1) (2020) 534–540.
- [30] F. Alzahrani, A. Hobiny, I. Abbas, M. Marin, An eigenvalues approach for a two-dimensional porous medium based upon weak, normal and strong thermal conductivities, *Symmetry* 12 (5) (2020) 848.
- [31] G. Veeram, P. Poojitha, H. Katta, S. Hemalatha, M.J. Babu, C. S. Raju, N.A. Shah, S.J. Yook, Simulation of Dissipative Hybrid Nanofluid (PEG-Water+ ZrO₂+ MgO) Flow by a Curved Shrinking Sheet with Thermal Radiation and Higher Order Chemical Reaction, *Mathematics* 10 (10) (2022) 1706.
- [32] V. Nagendramma, B.M. Rao, N. Sivakumar, G.M. Sarala, P. Durgaprasad, C.S.K. Raju, N.A. Shah, S.J. Yook, Energy dissipative MHD Cu-AA7072/water-based hybrid nanofluid flow over a perpetually moving slender needle, *Waves Random Complex Media* (2022) 1–13.
- [33] R. Kandasamy, V. Vignesh, A. Kumar, S.H. Hasan, N.M. Isa, Thermal radiation energy due to SWCNTs on MHD nanofluid flow in the presence of seawater/water: lie group transformation, *Ain Shams Eng. J.* 9 (4) (2018) 953–963.
- [34] R. Kandasamy, I. Muhammin, A.K. Rosmila, The performance evaluation of unsteady MHD non-Darcy nanofluid flow over a porous wedge due to renewable (solar) energy, *Renew. Energy* 64 (2014) 1–9.

- [35] F. Wang, U. Nazir, M. Sohail, E.R. El-Zahar, C. Park, P. Thounthong, A Galerkin strategy for tri-hybridized mixture in ethylene glycol comprising variable diffusion and thermal conductivity using non-Fourier's theory, *Nanotechnol. Rev.* 11 (1) (2022) 834–845.
- [36] Abu Bakar, S., Md Arifin, N., Khashi'ie, N.S. and Bachok, N., 2021. Hybrid nanofluid flow over a permeable shrinking sheet embedded in a porous medium with radiation and slip impacts. *Mathematics*, 9(8), p.878.
- [37] A. Sattar, Unsteady hydromagnetic free convection flow with Hall current mass transfer and variable suction through a porous medium near an infinite vertical porous plate with constant heat flux, *Int. J. Energy Res.* 18 (9) (1994) 771–775.
- [38] N.G. Kafoussias, N.D. Nanousis, Magnetohydrodynamic laminar boundary-layer flow over a wedge with suction or injection, *Can. J. Phys.* 75 (10) (1997) 733–745.
- [39] P.V.S.N. Murthy, S. Mukherjee, D. Srinivasacharya, P.V.S.S.S. R. Krishna, Combined radiation and mixed convection from a vertical wall with suction/injection in a non-Darcy porous medium, *Acta Mech.* 168 (3) (2004) 145–156.
- [40] H. Schlichting, J. Kestin, Boundary layer theory vol. 121 (1961).
- [41] C.S.K. Raju, M.D. Kumar, N.A. Ahammad, A.A. El-Deeb, B. Almarri, N.A. Shah, Non-linear dynamic movements of cnt/graphene/aluminum oxide and copper/silver/cobalt ferrite solid particles in a magnetized and suction-based internally heated surface: sensitivity and response surface optimization, *Mathematics* 10 (21) (2022) 4066.